# APPLICATION OF THE ELECTROOSMOTIC EFFECT FOR

# THRUST GENERATION

## by

## THOMAS EDWARD HANSEN

A thesis submitted to the

Graduate School-New Brunswick

Rutgers, The State University of New Jersey

In partial fulfillment of the requirements

For the degree of

Master of Science

Graduate Program in Mechanical and Aerospace Engineering

Written under the direction of

Professor F. Javier Diez

and approved by

_____

_____

_____

_____

New Brunswick, New Jersey

October, 2015

# ABSTRACT OF THESIS

## APPLICATION OF THE ELECTROOSMOTIC EFFECT FOR

## THRUST GENERATION

## by THOMAS EDWARD HANSEN

Thesis Director:

Professor F. Javier Diez

The present work focuses on demonstrating the capabilities of electroosmotic pumps, (EOP) to generate thrust. An underwater glider was successfully propelled by electroosmosis for the first time published - at 0.85 inches per second. Asymmetric AC voltage pulsing proved to produce higher flow rates then equivalent DC pumps for the same average voltage. Ultra-short pulsing proved 100 nanosecond rise times in EOP are possible, which surpassed published predictions by three orders of magnitude. Theories behind efficiency losses of high power EOP were investigated. Direct measurement of effective voltage at the face of a membrane is the most accurate way to determine voltage drop across the electrolyte of an EOP. Forced convection lowered efficiency of the EOP for low voltages by preventing capacitance charging, but proved to prolong pump life during high power application.

# Acknowledgements

I would like to thank Professor F. Javier Diez for allowing me to learn about and experiment with electrokinetics. Working in the Laboratory for Experimental Fluids and Thermal Engineering I was able to explore many disciplines of science ranging from chemistry to electronics. Prof Diez's guidance has helped me grow as a scientist by giving my projects direction and purpose.

I would also like to that my committee members, Professors of Mechanical Engineering at Rutgers University Kimberly Cook-Chennault and Shahab S. Zadeh, for volunteering their time to review my work.

In addition I would like to thank Joe Vanderveer and John Patrowski for always lending a hand when I needed to troubleshoot, fabricate, or measure just about anything. They had not only the tools, but also the knowledge, to send me in the right direction when I hit a difficult point in my experiments.

Thank you also to all the students I've worked with over my years at Rutgers. Arturo Villegas brought me up to speed on how to conduct research before I even tried my hand at electrokinetics. Thank you to Dan Piwowar and Andrew Miller for their input during the early stages of this research. A special thanks goes to Mena Tawfik and Marco Maia for their indispensable help in my projects from theory to application. Without them, much of what I have accomplished would not have been possible. In addition, thank you to Anirudh Thuppul, undergraduate researcher of the year, for volunteering his time to help the electrokinetics team whenever needed.

# Table of Contents

# List of Figures

# List of Tables

# List of Symbols

| Symbol | Description | Units |
|---|---|---|
| a | Pore Radius | m |
| $A_{el}$ | Electrode Surface Area | $m^2$ |
| $A_{noz}$ | Nozzle Area | $M^2$ |
| C | Capacitance | F |
| d | Electrode distance | m |
| D | Diffusion coefficient | $m^2s^{-1}$ |
| e | Electron Charge | C |
| $E_x$ | Electric Field | $Vm^{-1}$ |
| $F_x$ | Ion Drag Force per Volume | $Nm^{-3}$ |
| f | Frequency | Hz |
| F | Faradays Constant | $Cmol^{-1}$ |
| I | Current draw of Pore | A |
| $I_{elm}$ | Electromigration Current | A |
| $I_{adv}$ | Advective Current | A |
| $I_{noload}$ | Current with no membrane | A |
| L | Length | m |
| $L_e$ | Effective Channel Length | m |
| n | Moles of dissolved gas | mol |
| $\mathbf{P}_{in}$ | Power in | W |
| $\mathbf{P}_{out}$ | Power out | W |
| $\mathbf{P}_{pulse}$ | Pulse power draw | W |
| $\Delta P$ | Pressure Gradient | $Nm^{-2}$ |
| $P_x$ | Axial Pressure Field | $Nm^{-3}$ |
| Q | Flow Rate | $m^3s^{-1}$ |
| r | Radial Position | m |
| R | Electrical Resistance | Ω |
| $R_{el}$ | Electrode and Electrolyte Resistance | Ω |
| $R_{total}$ | Total Pump Resistance | Ω |
| t | Time | s |
| T | Temperature | K |
| Tr | Thrust | N |

| Symbol | Description | Units |
|--------|-------------|-------|
| u | Velocity | $ms^{-1}$ |
| V | Voltage | V |
| $V_{av}$ | Average Voltage | V |
| $V_{an}$ | Anode Voltage | V |
| $V_o$ | Overpotential Voltage | V |
| $V_{cat}$ | Cathode Voltage | V |
| $V_{dec}$ | Decomposition Voltage | V |
| $V_{eff}$ | Effective Voltage | $m^{-3}$ |
| z | Valence Number | |
| ε | Permittivity of Liquid | $Fm^{-1}$ |
| ζ | Zeta Potential | V |
| ρ | Density | $kgm^{-2}$ |
| μ | Viscosity | $Nsm^{-2}$ |
| ψ | Porosity | |
| κ | Inverse Debye Length | $m^{-1}$ |
| σ | Conductivity | $Sm^{-1}$ |
| $σ_∞$ | Bulk Electrolyte Conductivity | $Sm^{-1}$ |
| τ | Tortuosity | |
| $ρ_E$ | Charge Density | $Cm^{-3}$ |
| φ | Induced Potential | V |
| η | Efficiency | % |
| Λ | Sum of molar conductivities | $Sm^{-1}$ |

| Subscript | |
| --- | --- |
| - | negative charge |
| + | positive charge |
| an | anode |
| app | applied |
| cat | cathode |
| elm | electromigration |
| adv | advective |
| drive | driving |
| eff | effective |
| el | electrode |
| max | maximum |
| mem | membrane |
| noload | no membrane |
| noz | nozzle |
| o | overpotential |
| rem | remissive |
| total | total |

# Chapter 1.

# Introduction

## *1.1.  A New Frontier in Propulsion*

An emerging technology in oceanic data capture is the underwater glider. Underwater gliders, such as the Solcum glider shown in Fig. 1, are autonomous underwater vehicles (AUV) that are able to traverse hundreds, even thousands of miles across open ocean by simply changing their buoyancy. Forward motion is achieved by repetitive alteration between floating and sinking in conjunction with a set of wings, resulting in a large sinusoidal profile. Because the buoyancy change can be done with only slight volume change, the amount of energy required to run the glider is significantly less than a conventionally propelled AUV.
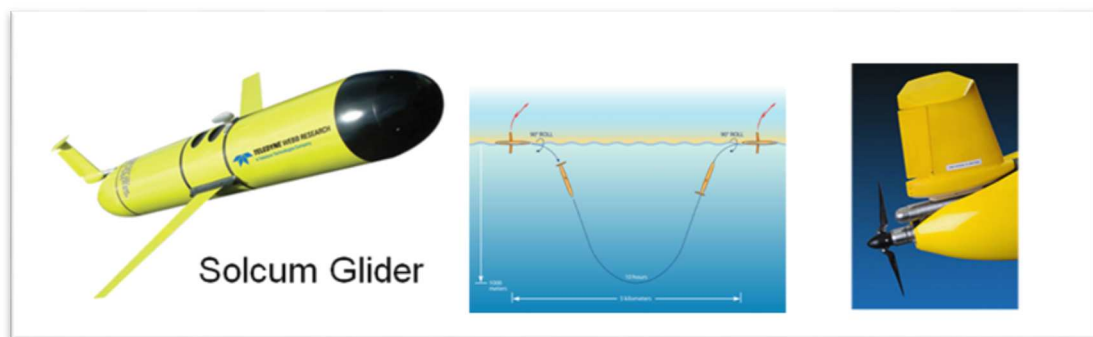


**Fig. 1. The Solcum Glider (left), glider's sinusoidal profile (center), and standard propeller thruster (right) [1]**

Gliders are an excellent choice for research in bodies of water with sufficient space to gain momentum. The large sweeping motion they require to operate effectively is on the order of a few hundred meters in length and depth [2]. Because the required area is so

significant, a small propeller is typically used to produce initial momentum following deployment or collision. Gliders are also fairly large in size, around 2 meters in length.

It is of interest of researchers and government, particularly the funding source for this study, to develop a shallow water glider with high efficiency and stealth. Shallow water gliders (<50m) will rely more heavily on their propulsion system to gain speed. Conventional thrusters use propellers which are bulky, cause wake, and have the potential of getting caught on seaweed or similar obstruction in shallow waters. Other conventional thrusters, such as impeller, piston pump, etc. all create wake noise and they all require bulky moving parts. An ideal thruster would require little volume and energy to operate while producing minimal wake.

Magneto-hydrodynamics pumps (MHD) are an alternative prospect for underwater stealth. MHDs were investigated in the early 1990's because they offered a propulsion system absent of moving parts. Little has been published on the matter in recent years, possibly because the unavoidable bubbles produced by electrolysis coupled with the extremely high magnetic field they require to operate rendered them unfeasible for practical application [3, 4].

A new frontier in displacement technology has been created by Micro pumps, which have undergone rapid growth in recent years [5, 6]. Micro pumps are small and relatively silent, but many cannot produce high flow rates, and are very sensitive to contamination. There is one pump that is not held back by these restrictions; the membrane based electroosmotic pump. Electroosmotic pumps (EOP) have high power to volume ratio, are absent of moving parts, are orientation independent, and are scalable - making them an ideal candidate for investigation as the next generation silent underwater thrusters for

small, and perhaps even large, vessels [7].

## 1.2. The Electroosmotic Pump

Electroosmotic pumps harness the electroosmotic effect to move fluid. The electroosmotic effect is the movement of fluid under electric field along a fixed surface [8]. EOP generally consist of one or many annular channels. These channels are submerged in an ionic aqueous solution, often an electrolyte. An electrode exists near the inlet and outlet so that an electric field can be applied.

EOP can be found in the fields of precision drug delivery, lab-on-a-chip processes, microprocessor cooling, chromatography, and water management in fuel cells among other applications [5, 6, 9, 10].Although they are widely used in these biological and thermal fields, they have not yet been explored for other applications where higher volume flows are needed. This is due to the faradic reactions occurring at the electrodes in EOP under high voltage (above 1V) and current (over 1mA) [11].

The goal of this study was to research and design an electroosmotic pump capable of generating thrust adequate for propelling a vehicle - an electroosmotic thruster (EOT).

## 1.3. Thesis Outline

EOP theory will first be explained in terms of its basic principles; output, input, and efficiency. The next chapter will cover efficiency losses in high power EOP; capacitance, faradic reactions, and voltage losses. An explanation of the EOP and its components along with the experimental setup and data acquisition will then be described. Efficiency

effects and membrane performance will be assessed before designing and testing a final

EOT. This study will be concluded by the performance of the first designed EOT.

# Chapter 2.

# Electroosmotic Pump Theory

Electroosmotic pumps, like all pumps, are classified by their ability to transport fluid with pressure and speed according to energy input. Power output of the EOP is determined by a number of fluid-surface interaction parameters [8]. In this chapter the basic background of electrokinetics, the field of study electroosmosis is defined and the theoretical parameters of electroosmotic pumping are described.

## *2.1. Background of Electrokinetics*

Electrokinetics refers to phenomena relating interaction between charged ionic solutions and a surface under the influence of an electric field [8, 12]. The particular interaction that makes electrokinetic flow possible is known as the electric double layer (EDL). Most surfaces spontaneously acquire a finite charge density $\rho_E$ when in contact with an aqueous solution [13]. The EDL exists naturally as the ions in an aqueous, or polar, fluid ionize, absorb, or diffuse away from a surface in which the fluid is in contact. A surface charge results as counter-ions are attracted to form a thin stationary layer called the stern layer [14]. Simultaneously, co-ions are repelled by excess charge, forming a dispersed layer known as the diffuse layer. This charge separation makes up the two components of a double layer which has a thickness relative to the fluids permittivity and ion concentration. The thickness of the EDL known as the Debye Length.

Under an electric field $E_x$ the EDL experiences a force $F_x$ in the field direction and sign of

the accumulated charge [8]

$$F_x = \rho_E E_x \qquad (2.1.1)$$

This force produces bulk movement through viscous drag. Fluid motion is classified to be either electroosmotic, in which fluid moves in reference to a fixed surface, or electrophoretic, in which individual particle surfaces move within the bulk. Electroosmosis is used for pumps because flow is continuous whereas electrophoresis is used for particle separation.

## 2.2. Pump Output: Flow, Pressure, and Thrust

The basis of electroosmotic flow in cylindrical pores for high zeta potentials $\zeta$ is outlined in Levine et al [15] where it resolves the low zeta potential values restriction [16]. Zeta potential refers to the electric potential across the shear plane which exists between the two layers of the EDL [8]. Using this electroosmotic theory, the maximum flow rate can be obtained. The velocity profile in a nano-pore of radius $a$ at radius $r$ in presence of both an axial pressure field $P_x = \Delta P / L_e$ due to the pressure gradient $\Delta P$ and axial electric field $E_x = V_{eff} / L_e$ due to effective voltage $V_{eff}$, both across the effective length of the channel $L_e$, assuming steady, low Reynolds umber flow and a 1:1 electrolyte is

$$u(r) = \frac{1}{4\mu}\left(a^2 - r^2\right)P_x - \frac{\varepsilon}{\mu}\left(\zeta - \varphi(r)\right)E_x \qquad (2.2.1)$$

where $\mu$ is the viscosity and $\varepsilon$ the permittivity of the liquid. The induced potential $\varphi(r)$ in a pore can be described using the solution to the Poisson-Boltzmann (PB) equation [15]. Then, the total volumetric flow rate of a channel can be obtained by integrating the velocity over the channel cross sectional area to find

$$Q = 2\pi \int_0^a ru(r)\,dr = \frac{\pi a^4 P_x}{8\mu} - \frac{\epsilon \zeta \pi a^2 E_x}{\mu} f \qquad (2.2.2)$$

where

$$f = \int_0^a \left(1 - \frac{\varphi(r)}{\zeta}\right)\frac{2r}{a^2}\,dr \qquad (2.2.3)$$

From (2.2.2) it can be shown that the resulting maximum flow rate occurs when pressure is zero

$$Q_{max} = -\frac{\epsilon \zeta \pi a^2 f}{\mu} E_x \qquad (2.2.4)$$

And maximum pressure when flow rate is zero

$$\Delta P_{max} = -\frac{8\epsilon \zeta f}{a^2} L_e E_x \qquad (2.2.5)$$

Electroosmotic flow was described in terms of a single channel but can be expanded by the total number of channels, or pores, in a membrane. For tortuosity $\tau = (L_e/L)^2$ and porosity $\psi$ of the particular membrane being used, the total flow rate is

$$Q_{total} = -\frac{\psi}{\tau} Q_{max} \qquad (2.2.6)$$

The ideal scenario for a high flow rate EOP as seen in (2.2.4) is high zeta potential and high electric field. Shallow pore depth is also ideal because as pore depth increases, resistance due to viscous drag increases while electric field, being relative to electrode spacing, decreases. The effect of reduced pore depth on flow rate for set applied voltage can be seen experimentally in Laser [17].

Thrust generated by incompressible flow through an orifice is the resultant force for change in mass at a velocity according to Newton's second and third laws:

$$Tr = u\frac{dm}{dt} = \rho A_{noz}u^2 = \rho\frac{Q^2}{A_{noz}} \qquad (2.2.7)$$

It is ideal then for the focus of this study, assuming properly a chosen nozzle, to have maximum flow rate through a minimal area nozzle $A_{noz}$. Because of the near-zero pressure involved in maximum flow rate, it is expect that choked flow will make nozzle selection very sensitive.

Rise time of electroosmotic pumps was theoretically calculated to be as low as 100μs [18]. Rise time has been investigated for use in actuators [19] but a maximum rise time has not been experimentally identified.

## 2.3. Pump Input: Voltage and Current

As seen in pump output theory, the ability of an EOP to generate flow is determined most effectively by the electric field across the channel that has a resistance R. Current draw of a pore $I$ is therefore governed by voltage input as in a typical resistive circuit. The total current draw in a channel is equal to electromigration current $I_{elm}$, and advective current $I_{adv}$ as outlined in [16]

$$I = I_{elm} + I_{adv} \qquad (2.3.1)$$

Where

$$I_{elm} = 2\pi\int_0^a \left[\sigma(r)E_x\right]rdr$$

$$ \qquad (2.3.2)$$

$$I_{adv} = 2\pi\int_0^a u(r)\rho(r)rdr$$

Following the steps outlined by [8] and [11], the maximum current draw $I_{max}$ for

electrolyte conductivity $\sigma_\infty$ is then

$$I_{max} = \frac{f\sigma_\infty A}{gL}V_{eff}$$
(2.3.3)

When $\Delta P=0$ and

$$g = \frac{f}{\frac{\varepsilon^2}{\mu\Lambda}\int_0^a\left(\frac{d\varphi}{dr}\right)\frac{2r}{a^2}dr + \int_0^a \cosh\left(\frac{ze\varphi}{kT}\right)\frac{2r}{a^2}dr}$$
(2.3.4)

where $g$ tends to unity at large $\kappa a$ values, that is, the pore radius is much larger than inverse Debye length $\kappa$. As shown in Eq. (2.3.3), the scaling of current with voltage in absence of additional effects is linear. Current is also relative to membrane properties in a similar manor to flow rate

$$I_{total} = \frac{\psi}{\tau}I_{max}$$
(2.3.5)

## 2.4. Efficiency

Electroosmotic pumps have hydraulic efficiency synonymous with other pumps as a ratio between power in and power out as

$$\eta = \frac{P_{out}}{P_{in}} = \frac{Q\Delta P}{IV_{app}}$$
(2.4.1)

Typically an EOP is analyzed based on maximum pressure and flow capabilities to simplify the testing process. For this, Chen et. al showed that efficiency can be obtained by the quarter of maximum performance [20]

$$\eta = \frac{Q_{max}\Delta P_{max}}{4IV_{app}}$$
(2.4.2)

# Chapter 3.

# Efficiency Loss

The efficiency losses in electroosmotic pumps that are generally acknowledged, then ignored in literature are capacitance [21], faradic reactions [11], and voltage drops across the pumps electrolyte prior to the channel entrance. These inefficiencies have an obvious effect on the pump performance by contributing to transient variations in current and flow [22] as well as subsequent pump failure [8]. These effects become increasingly important when input power is increased. The following chapter explains these effects along with methods of mitigating them.

## *3.1. Capacitive charging*

Early transient power consumption can be attributed to capacitive charging [21]. Capacitance $C$ due to EDL charging exists at the electrode with resistance $R_{ct}$ and can be described by an effective circuit [23] as
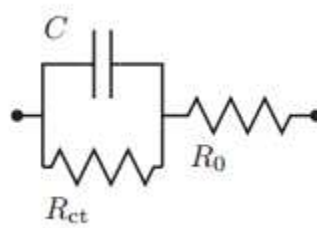


**Fig. 2. Equivalent circuit for electrode and electrolyte on either inlet or outlet side of pump [22]**

with $R_0$ representing the electrolyte resistance and the sum of all electrode and electrolyte resistance being $R_{el}$. Beyond the circuit in Fig. 2 is the electroosmotic channel. The

electroosmotic channel is considered, even though a double layer exists, to be purely resistive.

Charging of capacitance requires current draw that does not contribute to flow, as in

$$I(t) = C \frac{dV(t)}{dt} \qquad (3.1.1)$$

Therefore, it is a direct loss of efficiency. For most pumps this capacitance generally is small and requires milliseconds to charge [19]. However, larger pumps require more electrode surface area, which results in higher capacitance. It is expected that an EOT will require significantly greater electrode surface area; this will result in higher capacitance. Capacitive charging loss will then play a bigger role in EOT then in contemporary EOP applications.

## 3.2. Faradaic Reactions

A faradic reaction is defined as heterogeneous charge-transfer reaction occurring at the surface of an electrode [24]. In EOP, this reaction results in electrolytic bubble generation that not only requires energy to occur but also changes the fluid's properties. Dissolved gas can coat the electrode or membrane face, which reduces the effect of electric field [11]. In addition radical gasses and dissolved metals resulting from electrolytic reduction at the electrode can alter pH and conductivity of the fluid over long periods of operation. Changes in pH affect the zeta potential, which in turn affects flow rate and efficiency [25].

## 3.2.1. Chemistry of Electrolysis

When an electrode submerged in aqueous solution, as in an EOP, is brought to a voltage above its decomposition voltage, electrolytic reactions occur [12]. This value is generally around 1.2V [12], but has been published to be as high as 4.5V in EOP [26]. The goal of this study is to achieve high flow rates that involve potentials as high as 2kV. In this scenario, faradic reactions become a significant factor in overall pump performance. Following Tawfik and Diez [27], the number of dissolved gas moles generated at the electrode, $n$, is related to the current drawn by Faraday's law

$$n = \frac{It}{Fz} \tag{3.2.1}$$

where z is the valency number of ions of the substance (electrons transferred per ion), and F is the Faraday's constant. When using simple buffer solutions with low ion concentrations the half-reactions occurring on the surface of an inert electrode are

$$\text{Cathode (Reduction):} \quad 2H^+(l) + 2e^- \longrightarrow H_2(l)$$

$$\text{Anode (Oxidation):} \quad 2H_2 0(l) \longrightarrow O_2(l) + 4H_2(l) + 4e^-$$
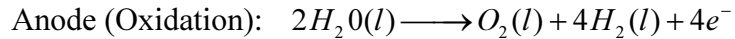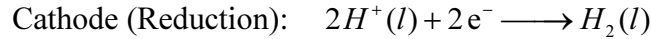
The dissolved $H_2$ and $O_2$ gasses formed at the electrodes build up until they reach a critical super-saturation. Beyond this threshold, bubbles will begin to form in nucleation sites such as dents, scratches, or cracks [28]. This super-saturation point has a timescale [27]

$$t^* = 0.19\pi z^2 F^2 D \left( \frac{I}{A_{el}} \right)^{-1} \tag{3.2.2}$$

where $A_{el}$ defines the surface area of the electrode with gas diffusion coefficient $D$. Considering there is a finite time required for generation, an optimal waveform can be

found in which bubbles are avoided [11].

For situations involving non-inert electrodes, complex electrolytes, or high salt concentrations - such as seawater, there will be a significant increase in production of other gasses and byproducts. It is of interest of this study to investigate methods to negate bubble nucleation to achieve long term stable high efficiency thrusters.

## 3.2.2. Methods of Mitigating Faradic Reactions

## Asymmetric AC Pulse

Most EOPs are designed to be operated under direct current (DC) voltage [5, 6]. Some pumps use symmetric AC signal with a unidirectional pump geometry [10]. Symmetric wave AC pumping allows for higher electric fields without electrolytic bubble generation. However, as the geometry of the pump is planar and would be difficult to implement into a large scale membrane-like assembly, this is unfeasible for a propulsion application. Conversely, an asymmetric square wave EOP can be built using a standard DC membrane assembly that allows for high flow rates without increasing bubble generation [11, 27]. Measurements will be compared in terms of average voltage, which is defined as

$$V_{av} = \frac{t_{drive}V_{drive} + t_{rem}V_{rem}}{t_{drive} + t_{rem}} \qquad (3.2.3)$$

where $t_{drive}$ and $V_{drive}$ are the time duration and voltage of driving pulse and $t_{rem}$ and $V_{rem}$ are the time duration and voltage of bubble remission pulse as shown in Fig. 3. It has been shown that using higher peak voltages with an asymmetric AC signal, a higher flow

rate will be produced than with a DC signal of equivalent average voltage [7]. A duty cycle pulsing also provides more constant flow rate [21].
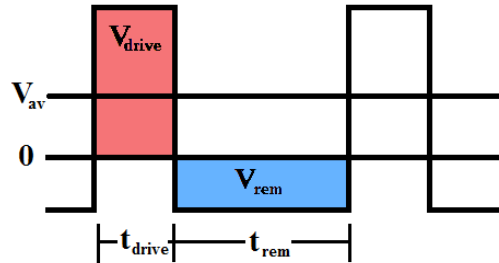


**Fig. 3. Relation between asymmetric AC pulsing and equivalent average DC voltage**

## Ultra-short DC Voltage Pulses

This study investigates bubble generation when power is applied for a very short amount of time followed by relatively long period of remission. On a nanoseconds scale, high voltage high speed pulsing may, if not completely eliminate bubble generation, delay bubble generation by increasing diffusion time relative to pulse width. This would result in equivalent average voltage application of thrust generating power with reduced bubble generation, therefore unlocking the potential of high power electroosmotic thrusters. A comparison between typical DC voltage, low duty cycle with equivalent average voltage, and ultra-short pulsing with equivalent average voltage can be seen in Fig. 4.
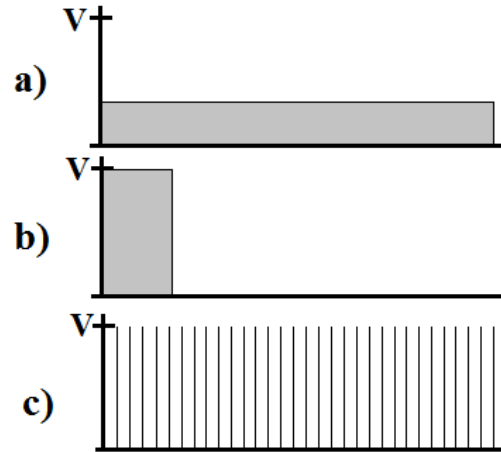
**Fig. 4. a) DC voltage, b) equivalent average DC voltage with low duty cycle, c) equivalent average DC voltage with ultra-short pulsing**

Capacitance must be as low as possible so that voltage can rise at ultra-short rates (3.1.1). Alternatively, current must be very high to charge quickly, on the order of tens of amps when capacitance and voltage are high. With this extra current draw considered, there is an additional power loss for high speed pulsing of frequency $f$

$$\mathrm{P}_{pulse} = CV_{app}^{2}f \qquad (3.2.4)$$

Fortunately, the capacitance of an electrolytic cell does not prevent its operation because it is in parallel as discussed in Section 3.1. It is then possible to raise the voltage in EOP to levels exceeding maximum rise time as discussed in Section 2.2. It is also of interest that not allowing capacitance to charge may actually result in even higher efficiencies for pulsing.

## Forced Convection

Gas super-saturation in (3.2.2) relies heavily on the diffusion coefficient. It is possible to use convection as a supplement for natural diffusion. These methods can include

agitation by stirring or sonication [29], removal and recombination of gasses [29, 30], and vacuum. These methods are investigated experimentally for their application. Agitation is counterintuitive for silence and space saving but gives insight to other aspects of pump performance.

Forced convection may also be desirable for high power EOP because it helps hold the local fluid temperature constant. Joule heating by the EOP increases fluid temperature, which makes output and efficiency measurement difficult as zeta potential increases with temperature [25, 31]. At very high voltages it is also possible for boiling to occur, which damages membrane, interrupts flow, and produces noise.

## Delocalization of Electrodes

Some pumps use chambers to separate electrodes from bulk fluid by use of Nafion membranes [32] or simple distance [33]. Although the research and development of an EOT may benefit from these separated chambers, it is the belief of the author that there is a better solution. Separated chambers require space, additional components, and accept the 'noise' produced by electrolysis.

## *3.3. Effective Voltage*

Electrolytic reactions and electrode separation cause voltage drop across the electrolyte within the EOP. Initial voltage drop occurs at the electrode due to the decomposition voltage [8]

$$V_{dec} = V_{cat} - V_{an} + V_o \qquad\qquad (3.3.1)$$

The value of decomposition for a given EOP configuration is the x-intercept of the I-V

curve. This value can sometimes be misinterpreted due to transient and nonlinear current draw at high voltages caused by faradic reactions.

The effective voltage, or voltage seen at the face of the membrane, can be directly obtained for a particular EOP setup though running it without a membrane [26]. Resistance of the electrode and electrolyte are then the slope of the I-V curve. Yao et. al combined these results and the experimental current to calculate the effective voltage as

$$V_{eff} = V_{app} - V_{dec} - IR_{el} \qquad (3.3.2)$$

$$R_{el} = \frac{V_{app}}{I_{noload}} \qquad (3.3.3)$$

Alternatively, Cao et. al. considered the decomposition voltage to be a function of pump resistance [34].

$$V_{eff} = \frac{R_{el}}{R_{total}} \left( V_{app} - V_{dec} \right) \qquad (3.3.4)$$

This assumes decomposition voltage is not constant. These equations are often cited, but have not been confirmed against a direct measurement as recommended [35]. The validity of the equations is important for assuring theoretical pump efficiency is obtained. The effective voltage can also be obtained through distance $d$, surface area of the electrode $A_{el}$, and bulk fluid conductivity $\sigma_{\infty}$

$$R_{el} = \frac{d}{A_{el}\sigma_{\infty}} \qquad (3.3.5)$$

# Chapter 4.

# Experimental setup

This chapter first describes the components of the EOP in this study. The pump test apparatus and experimental setup are then described. Design constraints for the final thruster are then outlined.

## *4.1. Membranes*

Early electroosmotic pumps were generally composed of packed silica beads [5]. They were capable of producing high pressures after long periods of time [36]. These pumps' efficiency and flow rate were low due to the thickness and high tortuosity of the silica bed. Sputtered glass frits are similar in design but fused. As they were more easily manufactured with different thicknesses and pore sizes, they became the membrane of choice for high flow pumps [8]. Glass frit membranes still had high tortuosity and thickness, so EOP researches started trying other membranes. Many pumps used in biomedical applications are based on planar microchannel fabricated from silicon using microfabrication technologies [37]. Similar micro fabricated pumps are used for heat management applications [17], but because they are planer and expensive to manufacture they are not feasible for this study. The following sections describe some of the other membrane types that may be feasible for EOTs.

### 4.1.1. Glass Micro Capillary Array

Glass micro capillary arrays (MCA) were obtained from INCOM USA. These arrays were made of borosilicate glass with a chemical composition of 72% $SiO_2$, 12% $B_2O_3$, 7% $Al_2O_3$, 6% $Na_2O$, 2% $K_2O$, and 1% CaO. They had a pore diameter of 10μm with a porosity of 60%, tortuosity of 1, and thickness of 1mm. The faces of the glass were polished by the manufacturer. Uniformity of the MCA can be seen in Fig. 5. MCA have become common for EOP because of their durability, pore size uniformity, and high silica content [22, 34].

Micro capillary membranes of similar dimensions were also purchased from PHOTONIS USA. These capillary arrays were made of laser etched lead glass, which has a lower silica content then borosilicate [38] but has higher strength and chemical stability. It is important to have high silica content as it results in high zeta potential [25].
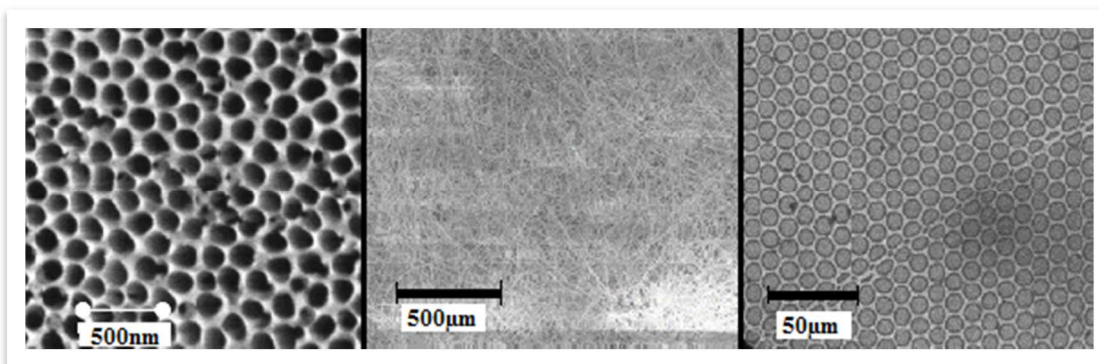


**Fig. 5. SEM image of membranes (left to right): AAO, Glass fiber, MCA**

### 4.1.2. Glass Fiber

Glass fiber membranes were purchased from Sterilitech because they are made of borosilicate glass, similar to MCA, but with smaller pore size and thickness, which should provide higher efficiencies [8]. In addition, they are significantly less expensive.

The glass fiber membranes are composed of packed strings as seen in Fig. 5.

## 4.1.3. Anodic Aluminum Oxide

Anodic aluminum oxide membranes (AAO) were obtained from Watman of GE Healthcare. They had a porosity of 30%, thickness of 150µm, and pore diameter of 200nm. AAO membranes are very common in high flow EOP because they are very thin while retaining high zeta potential [20, 35, 39]. $SiO_2$ coatings are common for these membranes to increase zeta potential [39].

## 4.1.4. Track Etched Polymer

Polymer membranes were used because of their effectiveness in EOP [40]. The polymer membranes chosen in this study were 200nm pore diameter, 10um thick, 10% open area track etched Polycarbonate (PC) and 200nm pore diameter, 2mm thick polyethylsulphoone (PES), both purchased from Sterilitech. A comparison of membranes tests is shown in Table 1.

**Table 1. Relevant information for membranes used in study**

| Geometry | Material | Supplier | Average Pore dia. (µm) | Thickness (mm) |
|---|---|---|---|---|
| Capillary Array | Borosilicate | INCOM | 10 | 1 |
| Capillary Array | Lead Glass | PHOTONIS | 10 | 0.5 |
| Fiber | Borosilicate | Sterilitech | 0.3 | 0.3 |
| Wafer | AAO | Watman | 0.1 | 0.05 |
| Track Etch | PC | Sterilitech | 0.2 | 0.1 |
| Track Etch | PES | Sterilitech | 0.2 | 0.2 |

## *4.2. Pump construction*

### 4.2.1. Housing

To assess the volumetric pumping capability of the membranes, a testing platform was designed capable of housing and supporting the membranes. This EOP housing is shown in Fig. 6. The membrane is glued into a thin support plate. The support was 3D printed using acrylic-like material.
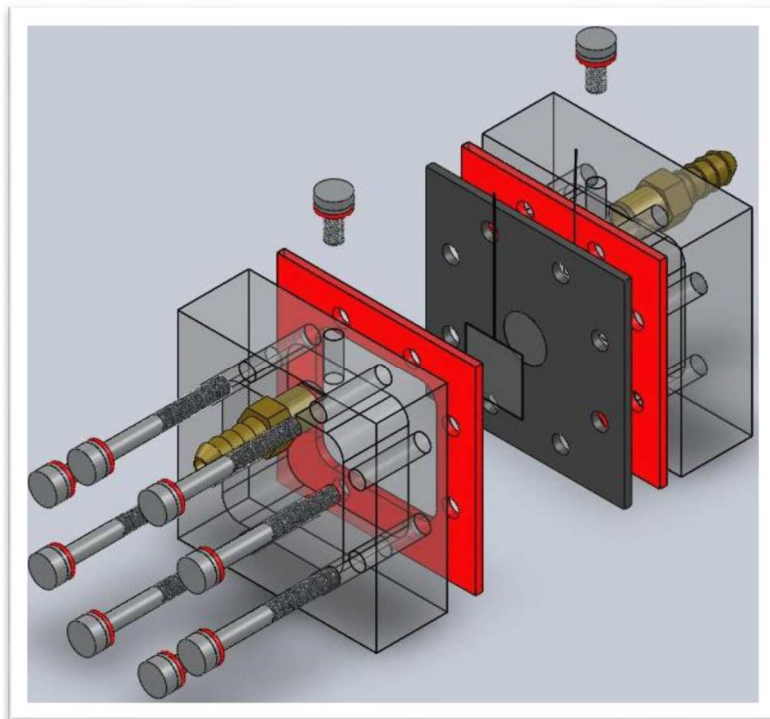


**Fig. 6. Basic assembly of EOP**

Membrane support assemblies were mounted in a machined acrylic enclosure fastened by aluminum bolts. The inlet reservoir of the enclosure had a large opening at the top. The outlet reservoir was sealable so that pressure and flow measurements would be more accurate. Experiments were performed on two different enclosure volumes; 10mL and

250mL. Inlet and outlet reservoirs had threaded channels so external reservoirs could be connected. The pump chamber was sealed using silicone rubber gaskets.

## 4.2.2. Electrodes

Platinum wire mesh (99.9% pure, Sigma Aldrich) was used as electrodes. Platinum was chosen as an electrode because of its high conductivity and low reactivity. Electrode spacing varied for experiments from 1.5mm to 5cm. Some experiments used platinum wire and platinum foil of the same quality. Gold, aluminum, and 316 stainless steel was compared for use in EOT.

Electrodes were also deposited on membrane faces to be used as reference electrodes for effective voltage measurements. Each membrane was first sputtered with 60nm of gold to serve as a test. The membrane with the highest sputtered quality had 20nm of chromium as an adhesion layer then 100nm of Platinum that served as reference electrodes as in [22].

## 4.2.3. Aqueous Solution

The primary solution used was Sodium Borate buffer. The buffer was made from Borax (Sigma Aldrich), Boric Acid (Sigma Aldrich), and deionized water such that the pH was 8.65. This particular buffer formulation was chosen because it is commonly used in other pump publications [8]. Based on the well documented EOP performance characteristics for varying molarity and pH this study used 1mM concentration buffer with conductivity of 35µS/cm. Conductivity and pH were confirmed using an Oakton 510 series meter.

## *4.3. Measurements*

The outlet of the EOP's housing was connected to an external reservoir with silicone tubing. This reservoir was placed on an A&D RJ200 balance to measure flow rate. Pressure readings less than 2psi were recorded by visual inspection of a manometer. For higher pressures, a WIKA 15psi compound gauge was used.

AC and DC signals used to generate electroosmotic flow were produced by a Tektronix AFG function generator with Thor Labs HVA200 amplifier. A basic diagram of the set-up is shown in Fig. 7. Pulse testing was done similarly using a DEI PVX4150 pulse generator powered by a Glassman FR3P100 DC source.
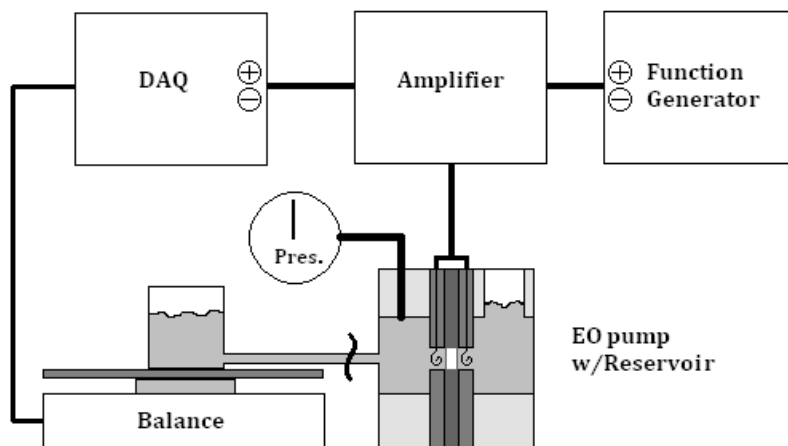


**Fig. 7. Experimental Schematic**

To measure current drawn by DC voltage, a RadioShack 46-Range digital multi-meter was used with supporting PC interface software. For AC experiments current was monitored using a DAQ card in conjunction with a LabVIEW program. Current consumption for pulse tests was recorded as the difference indicated on the Glassman

source with and without the pump connected. It was important to differentiate these values as the pulse generator requires power from the DC source to operate.

For effective voltage measurements, a Kiethley 6517B was used with a Matlab data acquisition program. All data was post-processed in Matlab.

Overall bubble generation by various methods was investigated by visual inspection of two parallel 316 stainless steel plates submerged in solution.

## 4.4. Thruster

A thruster was designed using lessons learned from all other research components of this paper. The ultimate goal of the thruster is to have proper balance of efficiency, durability, and thrust so that an underwater glider can be propelled. A dummy glider was first made to determine the thrust needed, as shown in Fig. 8. The dummy glider had similar dimensions to a micro glider designed and built by Marco M. Maia, which is also shown in Fig. 8. The back end of the dummy glider was threaded so different nozzles and flow rates could be tested. Flow was produced by a reservoir held at a height appropriate for simulating the pressure that is expected to be generated by the EOT.



**Fig. 8. Micro glider (left), reservoir with flow meter (center), dummy glider (right)**

# Chapter 5.

# Electroosmotic Pump Performance

The following chapter assesses characteristics of various EOP components and power application schemes that were tested in an effort to develop the best possible EOT. In the first section membranes are run through preliminary tests for their overall durability and pump feasibility. Experimental results for pump output and input under various power schemes are then analyzed. In the following sections electrolytic mitigation methods are assessed and effective voltage equations confirmed.

## *5.1. Preliminary Membrane Tests*

During preliminary tests it was found that membranes with small pore sizes suffered from degrading performance over time due to pore clogging as shown in below in Fig. 9.
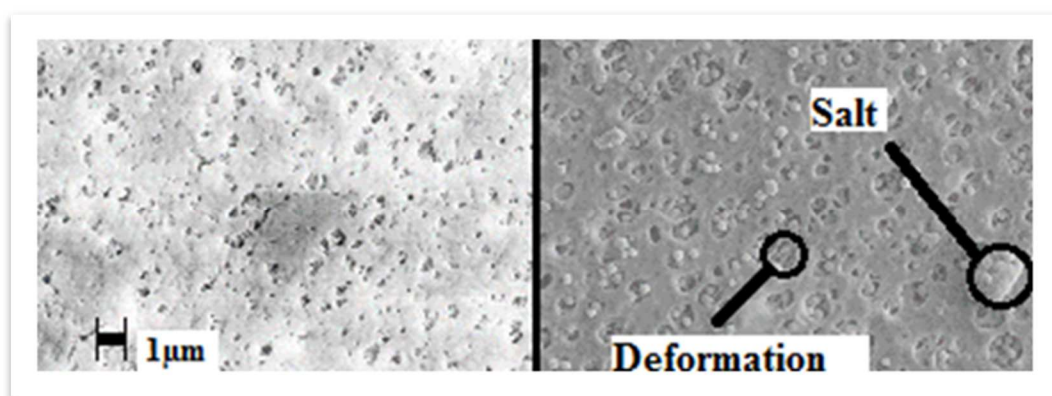


**Fig. 9. SEM image of a new (left) and PES membrane with debris and enlarged pores used (right)**

Fig. 9 also shows an expansion of the pores for the PES membrane. This deformation caused flow rates to be inconsistent. Deformation was found to be a problem for the other

flexible membranes; glass fiber and PC. Soft/flexible membranes also exhibited elongation of the center of the entire membrane in the direction of flow. After some time, the pore located at the crest of membrane elongation expanded enough to be considered a rupture, therefore rendering the membrane useless.

The AAOs were the thinnest membranes tested, as shown in Table 1. Because AAO membranes are perforated, thin, and rigid, they are very fragile. Rough handling caused them to fracture. They also suffered some heat damage when operated for too long or at high voltages (over 600V) as seen in Fig. 10.
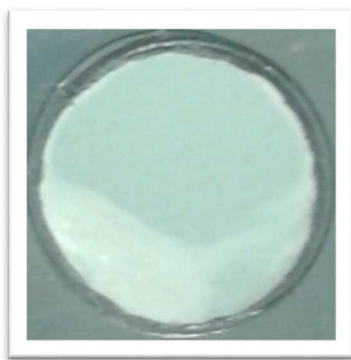


**Fig. 10. AAO membrane with heat damage in bottom left**

Only the glass MCA proved to last for long periods of time with no operational problems. Therefore, based on durability, the MCA was considered to be the best candidate for an EOT.

The effect of sputtering electrodes on the surface of the membrane was also evaluated as it would be important later in this study to deposit reference electrodes. Sufficient sputtering connectivity could not be achieved for the glass fiber membrane because its fibrous surface is discontinuous. The PC membrane was not an adequate electrical insulator so it failed at the initial power application of 50V due to arcing across the membrane. Sputtering of PES resulted in pores becoming clogged. AAO with sputtering

from Sterilitech (sputtered during manufacturing) were not clogged, but due to their thin nature they arced when applied DC voltage exceeded 600V (approximately 400V effective voltage).

The MCA did not have any problems with sputtering besides adhesion when current is applied. Gold does not adhere well to glass but the coating was sufficient enough to prove more sophisticated coatings could be used. The chromium and platinum layers were later successfully applied.

## 5.2. DC EOP

### 5.2.1. Flow rate

Flow rates for MCA, pore diameter of 10μm, and AAO, with pore diameters of 20nm and 100nm, can be seen in Fig. 11. Flowrate was highest for largest pore diameter membrane and lowest for smallest pore diameter. This is as expected, considering the large pore diameter increases flow rate as in Eq. (2.2.4). Flow rate for the MCA in this test was lower than preliminary tests by about 50%, likely because it became clogged. New AAOs were used for every test because they are inexpensive and degrade fast whereas the MCA was used repetitively due to its price and ability to be cleaned.
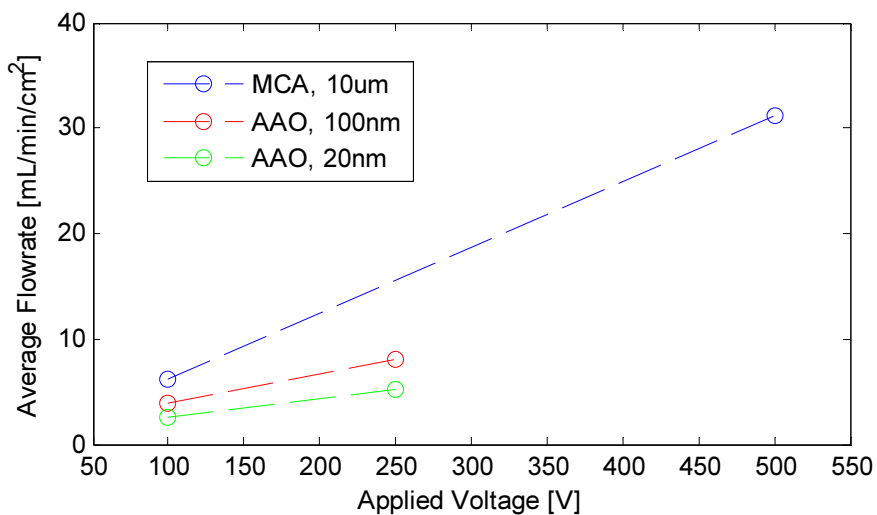
**Fig. 11. Flow rates for different pore diameter AAO and INCOM glass micro capillary array (MCA)**

In addition to being capable of high flow and high voltage, the flow rate measurement for the INCOM MCA was nearly constant with time up to 1.5kV. Fig. 12 demonstrates that a decline in flow occurred for only an instance of the high voltage test.



**Fig. 12. Flow rate for INCOM MCA as time elapsed for select voltages ranging from 100V to 1.5kV**

The drop in flow can be attributed to bubbles blocking the electric field. In another test lasting over 20 minutes the membrane recovered as bubbles dislodged from the electrode resulting in a quasi-steady flow rate during the entire pumping period.

The INCOM MCA was then compared to the PHOTONIS MCA with the same pore diameter 10µm and half pore diameter of 5µm. The INCOM mem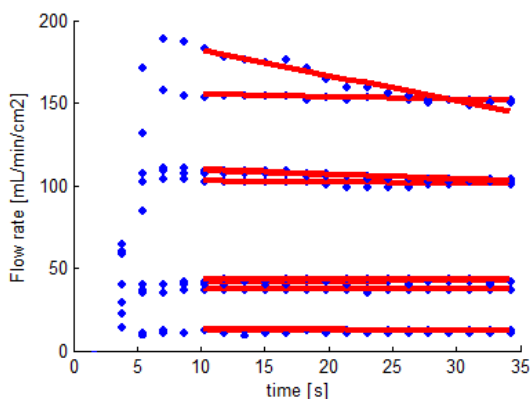brane had a higher flow rate, which was likely because of the higher silica content. This test also showed that flow rate was not significantly affected by moving from 10µm to 5µm pore size.

A new MCA was used with platinum foil electrodes to generate the highest flow rate per unit area seen for an EOP, as in Fig. 13. Results are compared to theoretical prediction with minimal voltage drop, warm water, and a zeta potential varying from -60mV to -120mV as seen in publication for borosilicate glass [8].
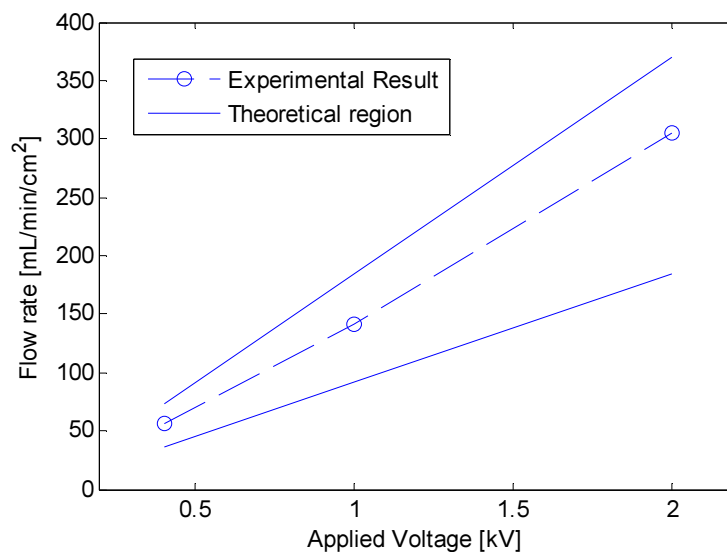


**Fig. 13. Flow rate for INCOM MCA with optimal electrode placement**

## 5.2.2. Pressure

Pressure was found to be relatively inconsistent unless the fluid was agitated. Results for maximum values are shown in in Fig. 14. For this test AAO membranes had to be mounted on a rigid mesh so that they did not deflect and facture when pressurized.
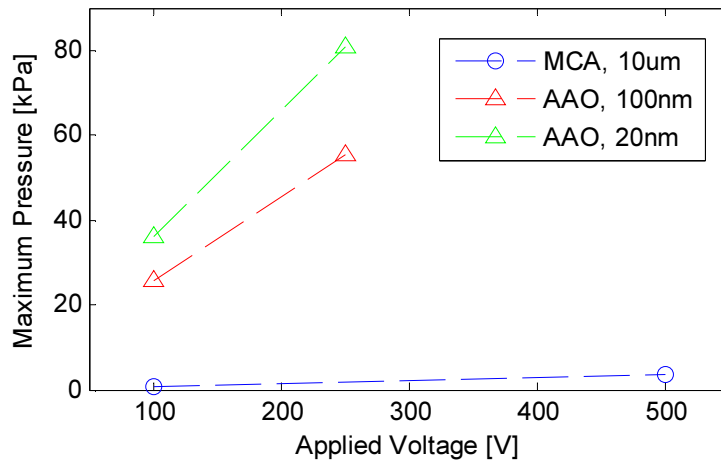
**Fig. 14. Pressure capabilities of AAO and INCOM MCA**

AAO was capable of higher pressures than the MCA due to smaller pore size as expected from Eq. (2.2.5). MCA has two orders of magnitude larger effective length as well as two orders of magnitude smaller pore size. Pressure is proportional to the square of the pore size, so it is the dominating factor in pressure. Pressure capability for decreasing pore size was further proven when comparing the two pore size AAOs in Fig. 14.

## 5.2.3. Thrust

The ideal membrane for its power output, as determined by maximum flow rate and pressure (2.4.1), was the AAO. Output capability is shown in Fig. 15.
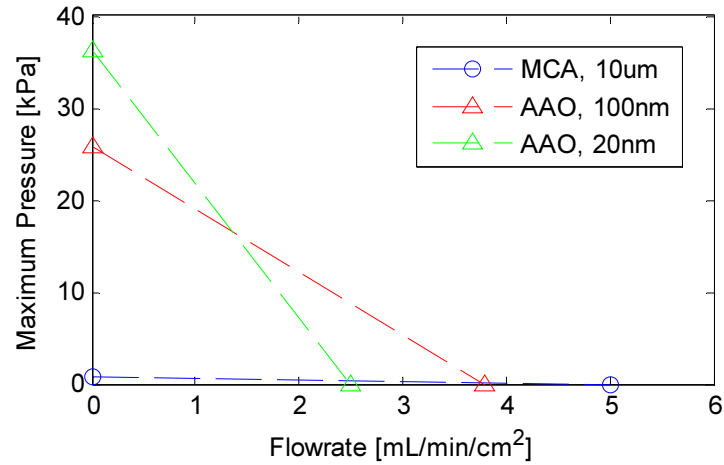
**Fig. 15. Output capability of AAO and INCOM MCA at 100V**

However, the flow rate is more important for thrust, as in Eq. (2.2.7); the MCA is the best choice for thrust.

The platinum foil electrode with a new 1cm$^2$ effective area INCOM MCA produced 14 milli-Newtons of thrust at 2.2kV applied voltage. This thrust is expected to be significant for moving a small vessel such as an EOT.

## 5.2.4. Current

Results were taken for current values after 15 seconds of operation when the current becomes relatively stabilized. According to Eq. (2.3.3), current draw should be similar between tests with similar output flow and fluid composition. This is shown in Fig. 16.
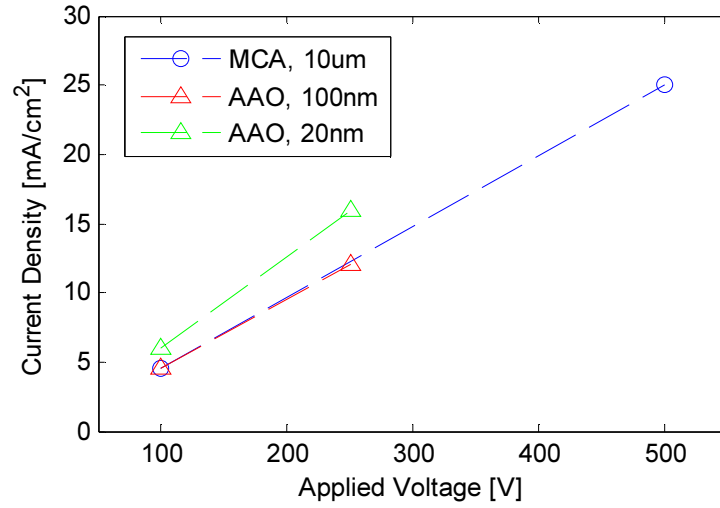
**Fig. 16. Current-voltage relationship for AAO and INCOM MCA**

In other experiments there was significant transience in current. This will be discussed in a later chapter.

## 5.2.5. Efficiency

Actual values for efficiency were obtained by using Yao's effective voltage method for the results of a separate set of experiments shown in Table 2.

**Table 2. Efficiency results for INCOM MCA and AAO**

|  | MCA | | AAO | |
|---|---|---|---|---|
| Applied Voltage | 100 | 500 | 100 | 250 |
| Effective Voltage | 48 | 240 | 27.5 | 50.4 |
| $P_{max}/2$ [Pa] | 800 | 4000 | 19000 | 37900 |
| $Q_{max}/2$ [m³/s] | 5.00E-08 | 2.08E-07 | 2.54E-08 | 5.33E-08 |
| Current [A] | 0.013 | 0.032 | 0.0063 | 0.0128 |
| Efficiency [%] | 6.26E-05 | 1.08E-04 | 0.28 | 0.31 |

Efficiency for AAO is orders of magnitude higher than MCA. This is because of the pressure capability of AAO. AAO also have more pore wall area which results in more effective use of electric field.

Efficiency as voltage increased was investigated for ideal thrust scenario from Fig. 13 as shown in Fig. 17. Efficiency drops for increasingly high voltage, which makes sense considering the significance of losses increases as mentioned in Chapter 3.



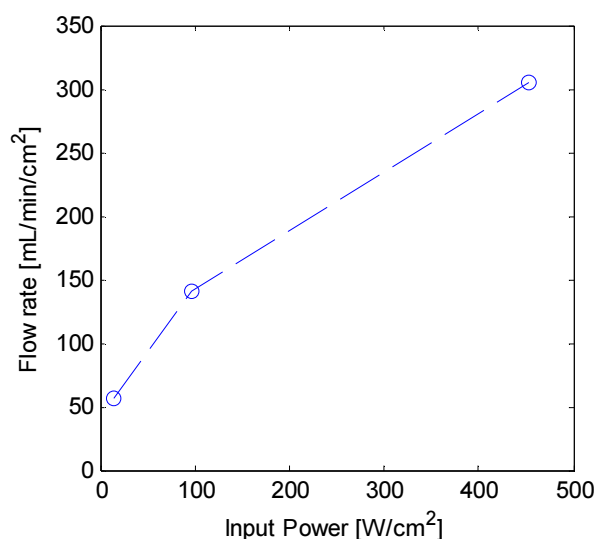**Fig. 17. Additional power draw of INCOM MCA when achieving high flow rate**

## *5.3. Asymmetric AC Voltage and Pulsing*

### 5.3.1. Flow Rate

Asymmetric AC voltage produced higher flow rate for the same average voltage as seen in Fig. 18. This is an interesting result considering flow rate is related to voltage linearly. The results imply that inertia of the fluid is important in AC asymmetric pumping.
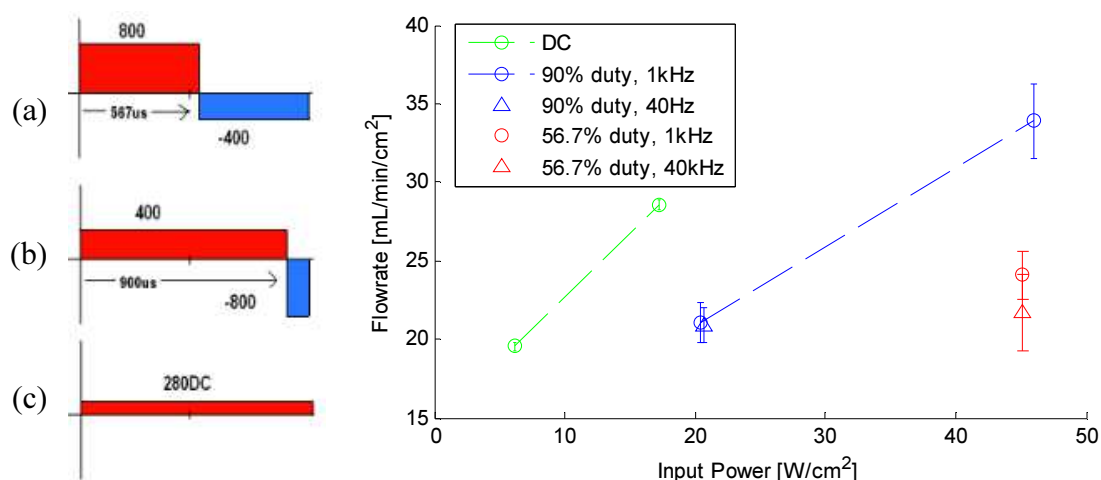
**Fig. 18. Asymmetric AC waveforms (left), flow generated compared to input power (right)**

Higher peak voltages resulted in higher peak flow values. Higher frequencies also produced a higher flow that would further point to inertia being a contributing factor. When the high voltage component of the AC wave was repeated more often, the inertial effects had a more significant contribution to flow.

Longer peak voltages, as in waveform (a) also required more power, as seen in Fig. 18, because they require more significant remission pulses to achieve the same average voltage. Overall, with power not being an issue, asymmetric AC pulsing allows for higher flow rates for the same average voltage.

Flow was then compared for 50% duty cycle high frequency pulses as shown in Fig. 19.
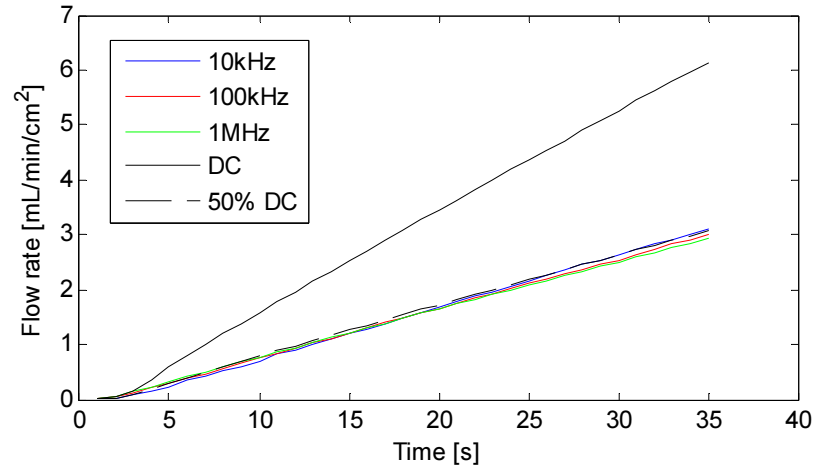
**Fig. 19. Displacement vs time for various input frequencies of 50% duty cycle single pulses**

It can be seen that 50% duty cycle consistently produces the same expected flow as 50% of DC at the same voltage at frequencies as high as 1MHz. This further proves frequency does not have a substantial effect of flow rate.

A 1MHz frequency with 50% duty cycle results in a 5μs pulse width. This outperformed published expectations [18] by two orders of magnitude. This is important, as ultra-short voltage pulses in the next experiment were expected to have 100ns rise times according to their 200 pulse width as seen in Fig. 20.



**Fig. 20. Rise and fall of pulse takes 200ns, but for simplicity flow and power usage will be calculated as if it were a 100ns square wave.**

Ultra-short pulsing was then tested and compared to single pulse DC of equivalent duty cycle as shown in Fig. 21.
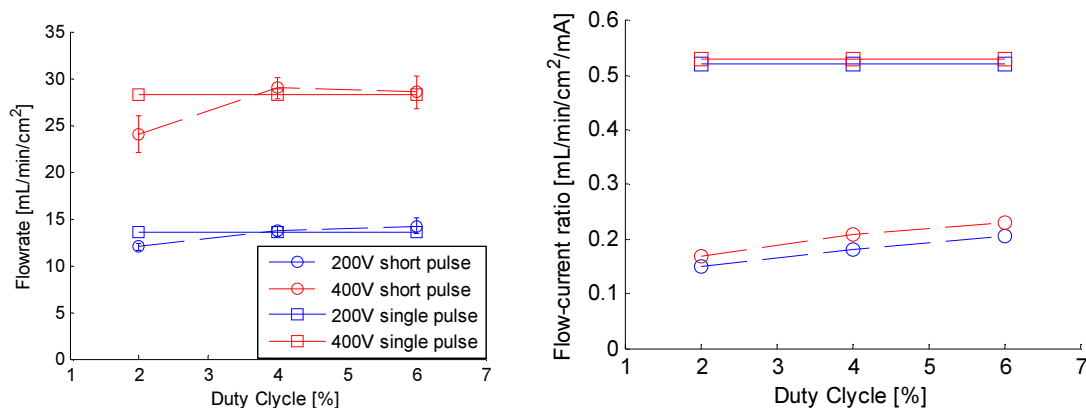
**Fig. 21. Flow rate and relative current draw for ultra-short pulsing compared to single pulse DC**

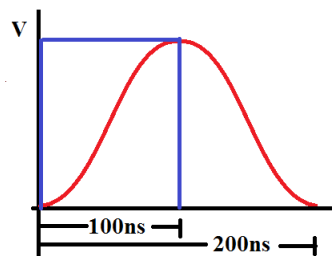Fig. 21 proves experimentally for the first time that the rise time for electroosmosis is significantly higher than predicted by mathematical models. There is some error in lower duty cycle due to data resolution. Current draw relative to the flow rate for ultra-short pulsing was higher than DC as expected. Continuous charging and discharging of the EDL was a waste of power as shown in Eq. (3.2.4).

## 5.3.2. Pressure

Pressure of AC square wave and pulsing was lower than DC. For situations that were not 100% duty cycle DC, there were periods when voltage was not present, or negative, causing pressure to decrease. Fig. 22 demonstrates that ultra-short pulsing produced a higher pressure at high voltage than single pulse, which makes sense as there is less time for back flow to gain momentum.
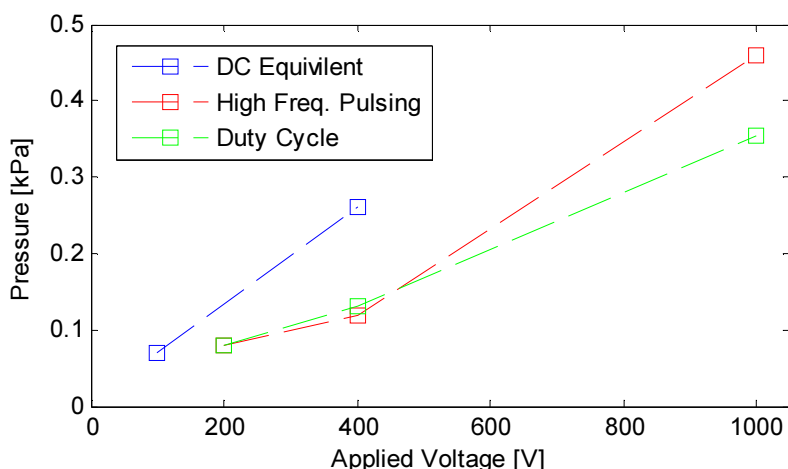
**Fig. 22. Flow rate and power usage for ultra-short pulsing compared to DC equivalent single pulse.**

Results shown in Fig. 22 are for MCA, which does not hold pressure well. AAO may show less difference between power schemes.

### 5.3.3. Efficiency

The diminished effectiveness of flow rate due to capacitive charging, coupled with significantly lower capability to generate pressure, resulted in significantly lower efficiency for waveforms alternative to 100% duty cycle DC.

## 5.4. Effects on Electrolysis

There was no obvious visual difference between all of the above waveform experiments when compared to the same average voltage. They all had bubble generation equivalent to the average DC voltage.

Attempts with other forms of bubble removal did not lead to any notable results either. Agitation by sonication was tested by submerging the EOP in a Branson 1510 sonic bath.

Ultrasonic vibration seemed to remove bubbles but did not affect flow as shown in Fig. 23. INCOM MCA was used for this test. The inlet and outlet reservoirs in this experiment were a few inches above the EOP because it had to be submerged. Therefore, there was a backpressure on the pump that caused flow to be lower than usual.
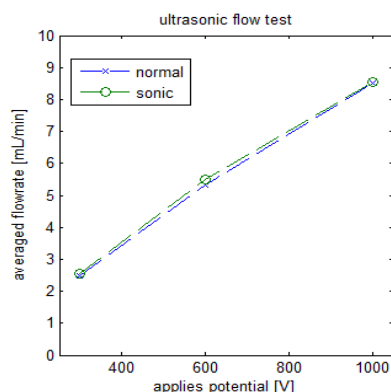


**Fig. 23. Effect of ultrasonic waves on EOP flow rate**

This test was done with external electrodes; it may be of interest if this test was redone for electrodes deposited on the face of the membrane. This method was abandoned as ultrasonic vibration did not have a substantial enough effect on flow to be considered for the final thruster design. The phenomenon that bubble removal by agitation did not affect flow is expanded on in the final section of this chapter.

Vacuum did not remove electrolytic bubbles from electrodes. A surfactant could be used to lower the fluids surface tension to help bubbles dislodge easier, but it is not feasible for use in the anticipated thruster application.

A recombination chamber was also tested [30]. This method was problematic as it required priming, proper orientation, and was only able to handle up to 5mA as literature suggests. It is expected a full scale thruster may require current on the order of a few amps. Recombination is therefore not feasible for final thruster design.

## *5.5. Transience and Effective Voltage*

In order to properly assess validity of various effective voltage equations, a comparison was done for wire electrodes distanced 1.5mm and 20mm from membrane, and also for foil electrode at 1.5mm. Results are as shown with direct measurement using a wire directly in front of membrane. Geometry refers to the use (3.3.5) for electrolyte resistance with Yao's method, current ratio is Yao's method with $R_{elec}$ found using blank membrane, and resistive difference is Cao's method.
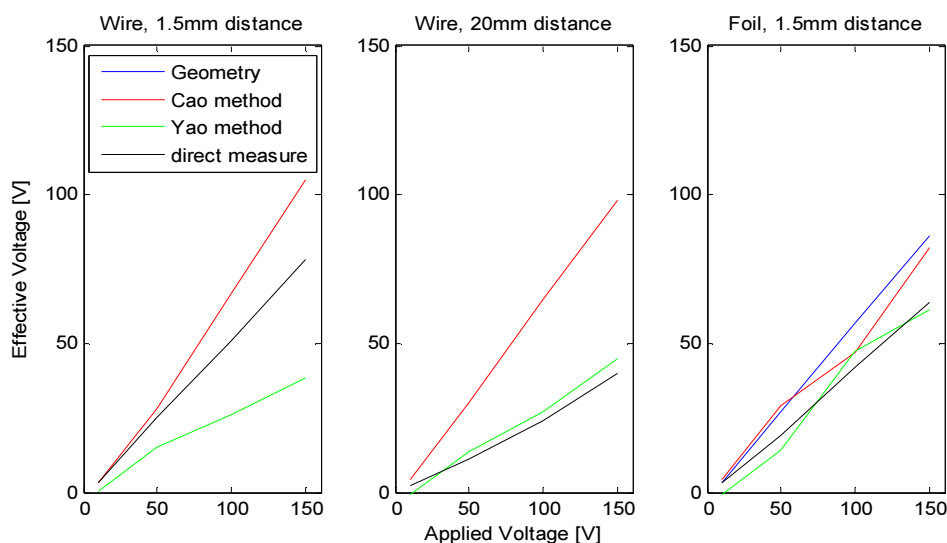


**Fig. 24. Effective voltage calculation by various methods for a close wire (left), large surface area foil (center), and far wire (right)**

Each method produced a different result. The geometry method resulted in completely wrong estimates, except for foil. Electric field is dependent on distance; the backside of the foil had a larger distance to travel than the front of the foil, which the equation does not consider. This could also be partly attributed to the non-linearity of fluid conductivity with distance as shown in Fig. 25.
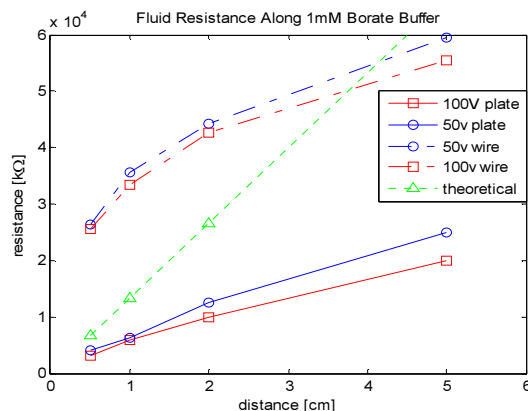
**Fig. 25. Resistance of buffer for electrodes at varying distances and surface areas compared to prediction from conductivity meter reading**

A problem with these measurements, as will be further explained, was due to the transient current of results. In order to properly use the equations, a current value needs to be chosen. The non-membrane scenario was the first to be tested. This was done for small and large apparatus with the results in Fig. 26 for a 5mm diameter hole and 1.5mm electrode spacing.
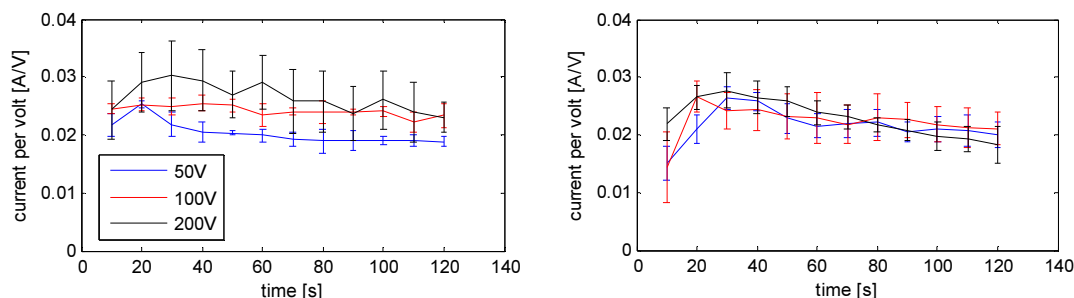


**Fig. 26. Current transience for 5mm diameter hole (left) and 1.5mm diameter hole (right) with no membrane present**

A test was run to investigate if general chamber size mattered; it did not. For both apparatus there was 20% average continuous fluctuation in current and 20% drop in current over 120 seconds as seen in Fig. 26.

A point of interest is that the drop was not more pronounced for higher power. This implies that increased bubble generation was not the culprit for current drop, but it was a

large capacitance as capacitance charge time does not change with voltage.

It was not clear from these experiments which value should be used for $I_{noload}$ in Eq. (3.3.3). Stirring was used in an attempt to remove any gas generation with results shown in Fig. 27.
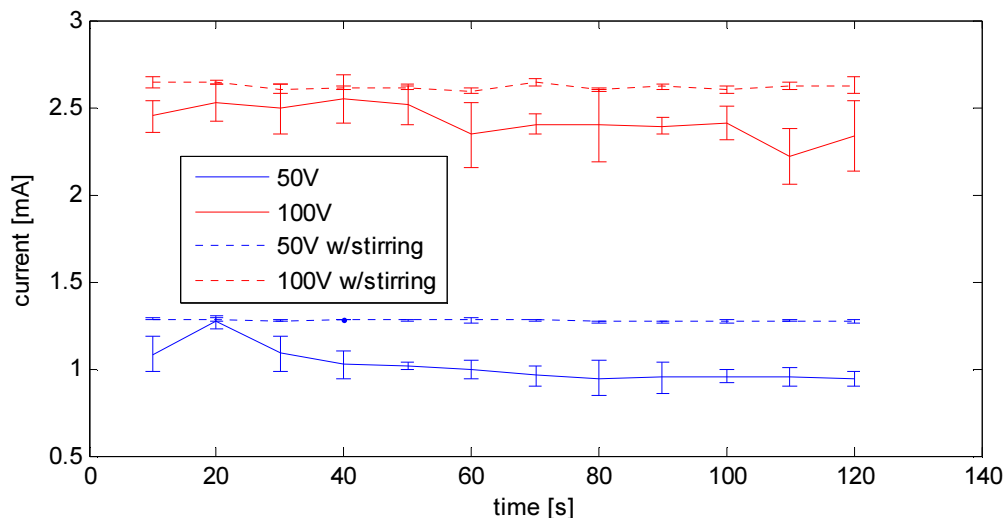


**Fig. 27. Current transience with and without stirring when no membrane is present**

Stirring removed current transience, but kept current high, this was a negative effect on efficiency. A simultaneous current and flow test was then taken using INCOM MCA at very high voltages to accentuate reactions.
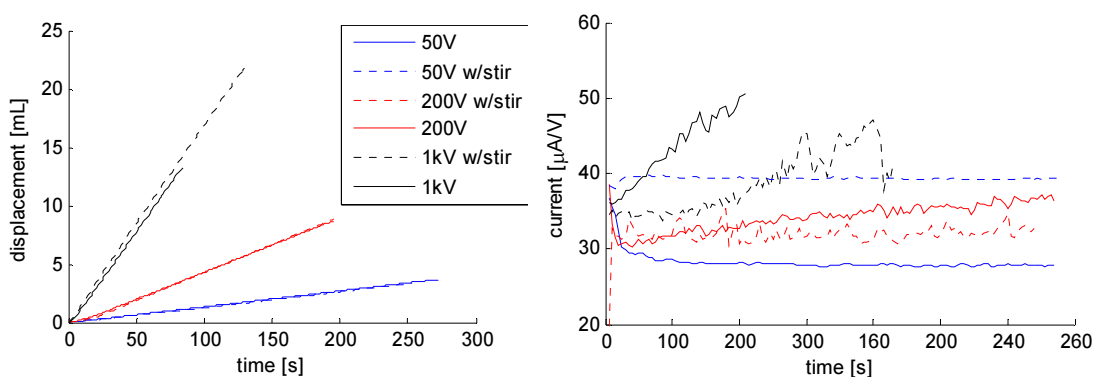


**Fig. 28. Transience of EOP displacement (left) and simultaneous current (right) with and without stirring at high voltage**

Stirring did not significantly affect flow, even at high voltages. Therefore, the effective

voltage would not be affected by stirring. Stirring did keep current from rising over time during higher voltage applications. Stirring therefore allowed high voltages to be run for longer periods of time because reactions were slowed. At lower voltages, it made the pump less efficient because capacitance can never charge.

It was interesting to see that the initial drop in current was less significant as voltage increased. This can be due to electrolysis destroying EDL at the electrode surface that effectively reduced capacitance. Also, the 1kV test led to boiling when stirring was not used.

The previous experiment shows that current after transience is the correct $I_{noload}$ for use in the effective voltage equations. To further investigate validity of the effective voltage equations, voltage was applied 1.5mm from INCOM MCA and read by electrodes deposited on the face of the membrane as seen in Fig. 29. Stirring did not significantly change effective voltage, as expected because they produced the same flow rate. This test was then run for a lower voltage, 10V, so current was low enough to be applied directly to the face of the membrane. The resulting current can also be seen in Fig. 29.
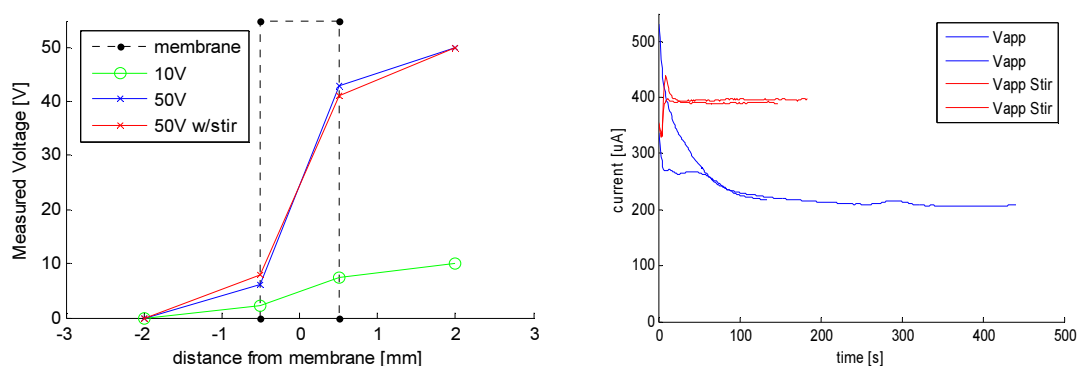


**Fig. 29. Effective voltage reading from reference electrodes deposited on membrane face (left) and resulting current transience for 10V case (right)**

Reference electrodes showed a voltage of 5.1V across the membrane, so 5.1V was then

applied directly to the face of the membrane. Results of the current draw for that test are shown in Fig. 30.
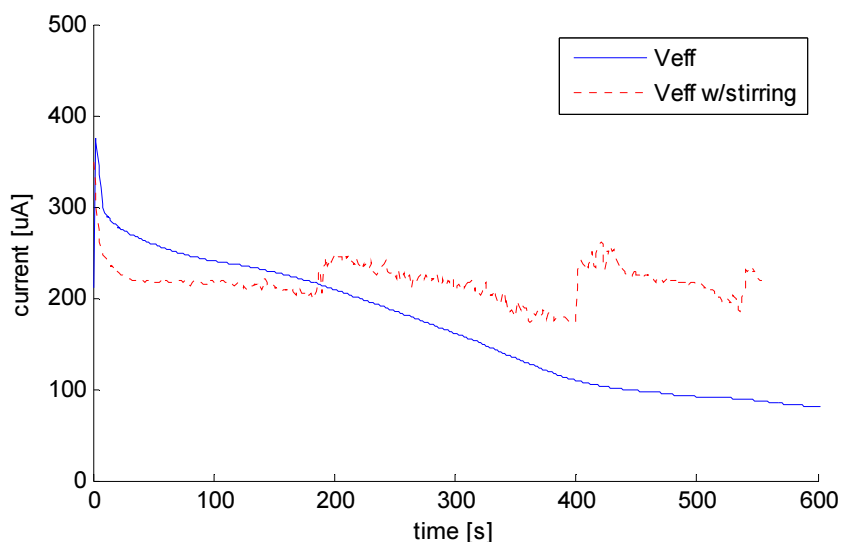


**Fig. 30. Current transience when voltage is applied directly to electrodes deposited on the membrane's face**

Results confirm that reference electrodes correctly read voltage at the face of the membrane because results in both scenarios are about 250µA. Fig. 30 data showed that without stirring, if voltage is applied directly, current continued to drop over long periods of time. Apparently stirring was incapable of effecting capacitate current when voltage was applied directly to the face because the initial drop was still present, unlike in Fig. 29.
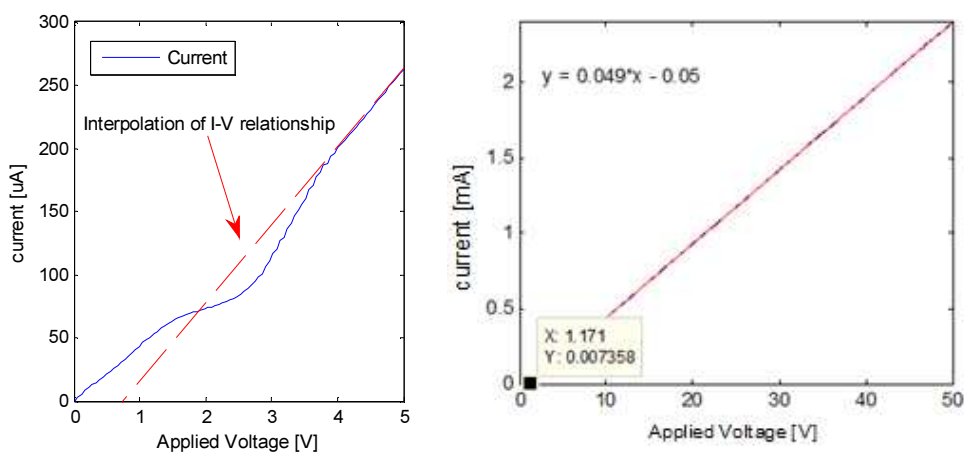
**Fig. 31. Identifying decomposition voltage using low voltage ramp (left) and current-voltage relation in experiments (right)**

$V_{dec}$ was found using the I-V line as shown in Fig. 31 to be around 1V, which agrees with published theory. Notice also in Fig. 31 there was a bend in the current during voltage ramp. This bend is explained in [41] as EDL charging. By ramping voltage up to 5V, the x-intercept predicted by Yao to be the decomposition voltage, was not necessarily the voltage needed to be exceeded before conduction occurred. As flow rate is a function of electric field, to say that a voltage needs be exceeded was somewhat misleading and should be further investigated.

All together, the theories did not match as well as a direct measurement. No-load current is 360µA. Yao's method for 10V applied resulted in an applied voltage of 2.4V instead of 5.1V. Cao's method predicted 5.6V, which was much closer to the value found by direct measurement. For low voltages, $V_{dec}$ made a significant impact. Also, the $V_{dec}$ also existed at the face deposited electrodes used in direct voltage measurement. It may be that there was a secondary decomposition that occurred that should be added to the equation.

In addition, the resistance measurement, $R_{el}$, in absence of membrane had an additional 1mm of fluid separation. Because the total electrode separation was 6mm, this 1mm error can cause $I_{noload}$ to be incorrect by 17%. Also, previous tests have demonstrated that current was not perfectly linear as in Fig. 25. Future work in effective voltage should take these factors into consideration.

Ideally this test would have been run at higher voltages. Unfortunately, high voltages resulted in face deposited electrode failure. Future work should use significantly thicker coating done by E-beam deposition.

Tests were also performed at a far distance of 5cm. Results as shown in Fig. 32 give

evidence that capacitance has much less impact at far distances.
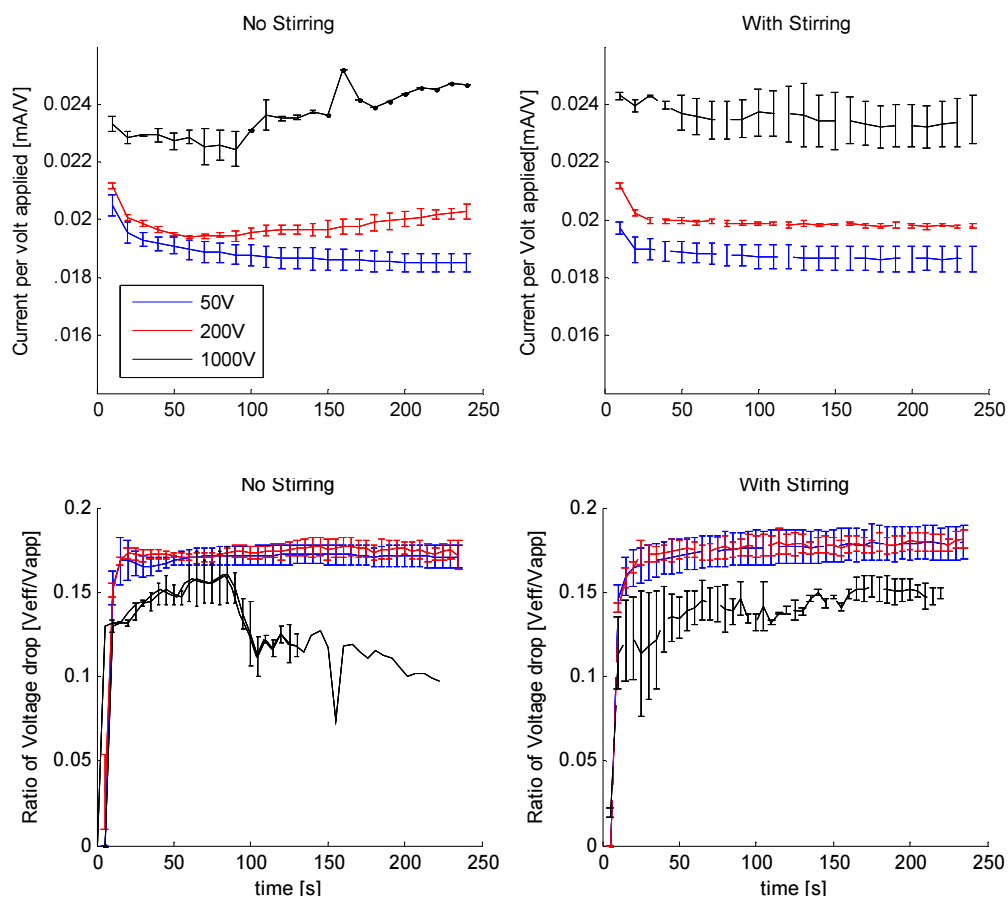


**Fig. 32. Transience of current draw (above) and ratio of effective voltage (below) for applied voltage with no stirring (left) and stirring (right) when electrodes are far from membrane**

Even for far electrodes, stirring appears to help reduce current rise at high voltage.

# Chapter 6.

# Design and performance of Electroosmotic Thruster

By incorporating what is learned by output, efficiency, and reliability research, an EOT was designed for optimum thrust and tested.

## *6.1. Design*

### 6.1.1. Membrane

The best membrane for an EOT is one which can produce the highest thrust without failing. As stated in Chapter 5, the MCA was the most reliable and produced highest thrust especially for high voltages. For these reasons, it was chosen for use in the final thruster.

Ideally, the pressure capability of the AAO would make it more effective at producing high thrust when a nozzle is present. AAO, though, could not be trusted to resist fracture. If a very thin, very rigid membrane support could be glued to AAO it would be more feasible.

Polymer and fiber membranes were rejected because as stated previously their deformation made then unreliable.

## 6.1.2. Electrodes

Platinum foil, gold sputtered plastic, and aluminum foil were first compared. The used membranes are shown in Fig. 33.
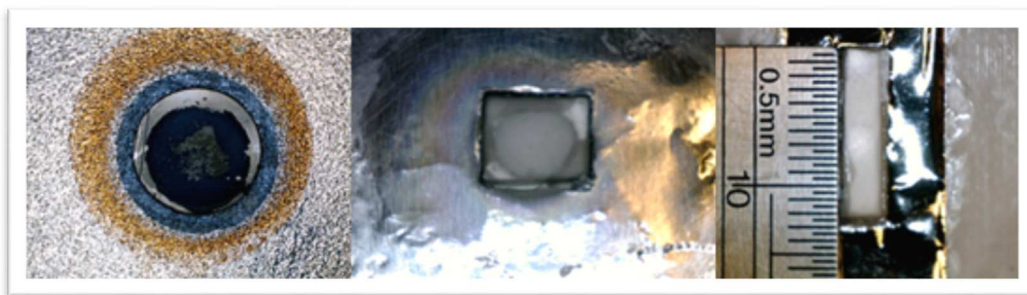


**Fig. 33. Electrodes compared for use in EOT; Gold sputter (left), Aluminum (center), and Platinum (Right)**

Gold and aluminum experienced reactions at high voltage and therefore produced lower flow rates as shown in Fig. 34.
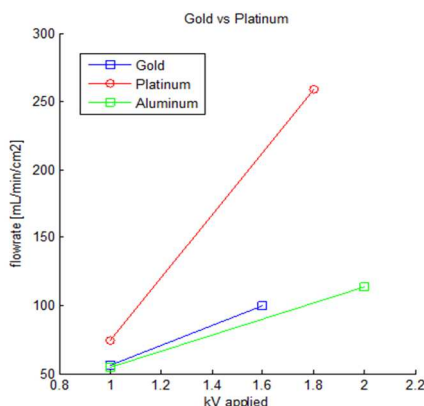


**Fig. 34. Flow rates for various electrodes**

It was not economically feasible to use platinum foil for the large scale thruster. 316 corrosion resistant stainless steel was experimented with as an alternative as suggested by Yao et. al. [8]. The stainless steel gave comparable results to platinum. Rust accumulated over time especially when high voltages were used, but the flow rate was appropriately constant.

Low levels of corrosion were acceptable for the thruster given that early models would only be operated for a short period of time. Electrodes in the final design would have to be replaceable in case more experiments were needed.

## 6.1.3. Fluid

Thrust generation in seawater is the ultimate goal of this research, but to keep the final test consistent with prior experimentation, 1mM borate buffer was be used. As proof-of-concept, a small vessel, shown in Fig. 35, was first moved with only 2.5cm$^2$ MCA, stainless steel electrodes, and small nozzle.
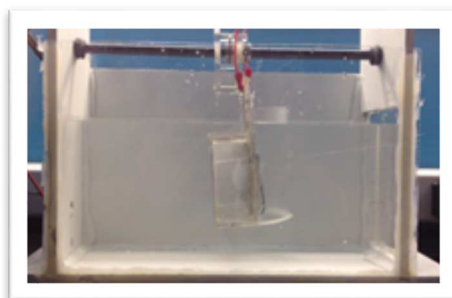


**Fig. 35. Small thruster on linear bearing to prove capability of MCA EOT with stainless electrodes to create sufficient thrust**

This test was operated at 2kV, which was about 10mN of thrust.

Near 100 gallons of 1mM Borate buffer, the same buffer used in all tests, was made in a large fish tank for testing of the final design.

## 6.1.4. Thrust Required

According to tests with the dummy glider, 140mN of thrust is required to move the vessel. Ideally this could be achieved using a very small amount of membrane at high voltage, but problems arise for high voltage as the current draw combination becomes

seriously dangerous. High voltage also results in lower efficiency, chance of boiling, and high electrolytic gas generation which effects buoyancy of the glider and defeats the purpose the silent operating thrust that is expected of the EOT.

Because flow rate is linear with voltage, it was more sensible to increase membrane area to a maximum to reduce voltage requirements while achieving the same flow rate. The largest MCA available within the study's time and cost constraints was $100cm^2$. According to thrust equation and prior results, thrust per volt for $100cm^2$ membrane through a 0.12 inch diameter nozzle was 0.66mN/V. Therefore the voltage required to produce adequate thrust would be about 250V. This voltage would require approximately 4A.

## 6.1.5. Power source

To ensure successful results, a battery assembly was designed to provide double the thrust required to move the glider. Using hobby grade Lithium ion batteries from Turnigy, a 550V, 10A battery pack was constructed. The battery pack was made to replace the glider's original power supply. Power was initiated by a laser triggered relay controlled by Arduino. The design, construction, and troubleshooting of battery pack and circuitry of this battery assembly, shown in Fig. 36, was led by Marco Maia.
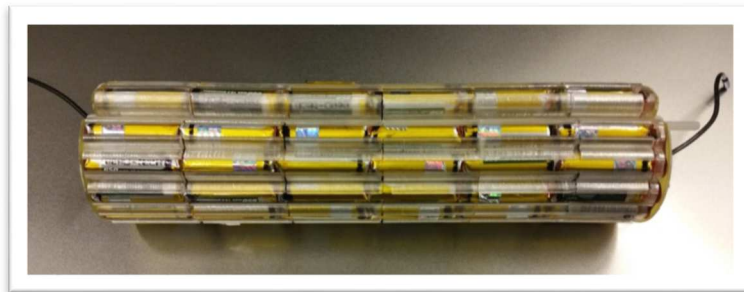


**Fig. 36. 550V 10A battery pack for use in micro glider**

## 6.1.6. Housing Geometry

The thruster construction had to conform to the glider shape and be as compact as possible. To achieve this, the membrane was split into four pieces and assembled so that they pumped in parallel while being linearly oriented. Electrodes were spaced so they could be as close as possible while allowing hot gas-saturated water to escape without damaging the membrane or blocking flow. Construction geometry can be seen in Fig. 37.
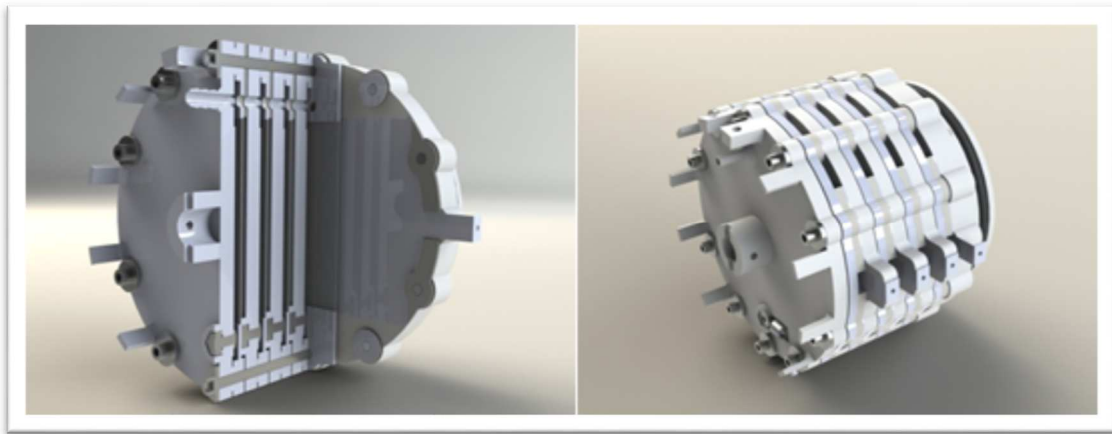


**Fig. 37. Construction of EOT; cutaway to highlight parallel pumping chambers (left), exterior showing inlet connections and bubble exhaust ports on top (right)**

The housing was 3D printed on an OBJET printer using Acrylic-like material. Gaskets were printed on the housing from neopreme-like material. 304 Stainless steel bolts were used for fasteners. All electrical connections were sealed using Loctite 5 minute epoxy.
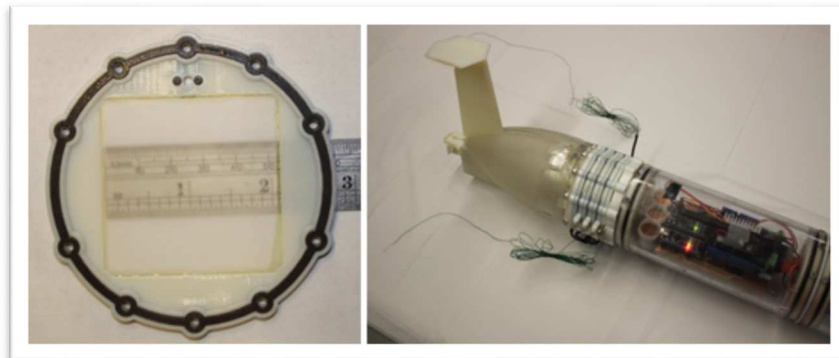


**Fig. 38. Individual EOT membrane section (left) and EOT thruster on glider (right)**

## *6.2. Results*

Nozzle sizes were tested for the voltages allowed by device size constraints using a camera and graduated cylinder, shown in Fig. 39.
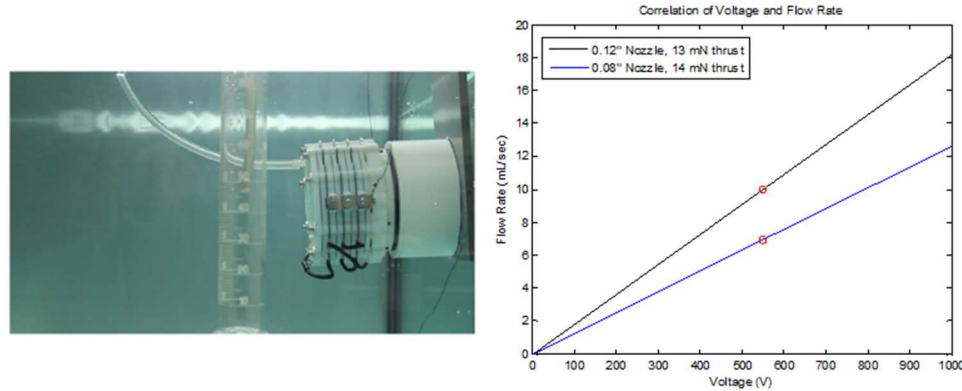


**Fig. 39. EOT output test with graduated cylinder (left) and results (right)**

Actual thrust generation was an order of magnitude lower than expected. This was believed to be due to small short circuits that occurred from inadequate adhesion of glue on the housing material. Also, not all gaskets achieved proper seal because of the flexibility of the material, which was significantly less rigid then typical acrylic. Heat resistance of the 3D printed material was also very low; the recommended limit was 56ºC. It is imperative that future housings are constructed of machined acrylic or similar material.

The final tests with the glider used an equivalent Turnigy Lithium polymer external battery source. The wires used to connect the external battery significantly restricted the mobility of the glider, which impacted the results of the experiments.

The glider moved at speed 0.85 inch per second for 10 second bursts. Although this result was slower than expected, it was a success none the less.

**Fig. 40. Glider with EOT installed; final test**

Future models should involve MCA with pore and thickness closer to that of AAO. An ideal pore size of around 2μm should be used as opposed to 10μm according to [8] but is not currently available on market. Custom manufacturing of membrane as done in [22] would be ideal, but was not economically feasible for this study. Smaller pore size would also produce higher pressures, allowing for smaller nozzles and preventing possible backflow in regions of lower electric field.

A purification system and trickle charge super capacitor will be necessary for the final application. The purification should have the ability to reduce salinity and decontaminate incoming water. The super capacitor will gain charge slowly from system batteries and discharge when thrust is needed.

# Chapter 7.

## *7.1. Conclusion*

With proper membrane selection an EOT can be designed. The glass micro capillary array used in our experiment was the only membrane in the study that did not suffer from permanent degradation under high voltages lasting more than a few minutes. The glass array's success could be linked to its large pore size, rigid construction, and high zeta potential. The glass array also produced the highest flow rate published for an electroosmotic membrane at 306mL/min/cm$^2$ for 2kV using aqueous buffer. It was observed that when using an asymmetric square wave signal, the flow rate can be increased while producing equivalent bubble generation to same average DC voltage. Ultra-short high voltage pulsing proved to produce flow rates with 100 nanosecond rise time which is three orders of magnitude higher than published numerical prediction. Forced convection lowered efficiency of pump for low voltages by preventing capacitance charging, but prolonged pump life at high power application. The effective voltage equation in which the decomposition voltage was related to pump resistance, as presented by Cao et. al, proved to be the most accurate for low voltage measurements. Direct measurement is the most effective way to determine true effective voltage. A thruster was developed capable of moving an underwater glider at 0.85 inches a second. Further work should be done on eliminating bubble generation so that pump can run undetected. The next generation thruster should be made in similar style with stronger, heat resistant materials and a smaller pore size membrane.

# References

[1] "TELEDYNE WEBB RESEARCH," Teledyne Technologies Incorporated, 2010. [Online]. Available: http://www.webbresearch.com/slocumglider.aspx. [Accessed May 2015].

[2] S. L. Wood, "Autonomous Underwater Gliders," in *Intelligent Underwater Vehicles*, Vienna, Austria, I-Tech Education and Publishing Kirchengasse, 2009, pp. 505-530.

[3] K. Tempelmeyer, "Electrical Characteristics of a Seawater MHD Thruster," David Taylor Research Center, Bethesda, MD, 1990.

[4] S. H. Brown, J. S. Walker and N. A. Sondergaard, "Propulsive Efficiencies of Magnetohydrodynamic Submerged Vehicular Propulsors," David Taylor Research Center, Bethesda, MD, 1990.

[5] D. Laser, "A Review of Micropumps," *Journal of Micromechanics and Microengineering,* vol. R35, no. 14.6, 2004.

[6] P. Woias, "Micropumps- past, progess, and future prospects," *Sensors and Actuators B,* vol. 105, no. 1, pp. 28-38, 2005.

[7] T. E. Hansen, M. E. Tawfik and F. J. Diez, "Application of the electrosmotic effect for thrust generation," in *ASME 2014 4th Joint US-European FLuids Engineering Division Summer Meeting*, Chicago, 2014.

[8] S. Yao, Electroosmotic Pump Technologies: Theory, Design, and Demonstration, Saarbrucken: VDM Verlag Dr. Muller Aktiengesellschaft & Co. KG, 2008.

[9] X. Wang, C. Chang, S. Liu and S. Wang, "Electroosmotic pumps and thier applications in microfluidic systems," *Microfluidics and Nanofluidics,* vol. 6.2, no. 145, pp. 145-162, 2009.

[10] C. Huang, M. Z. Bazant and T. Thorsen, "Ultrafast high pressure AC electro-osmotic pumps for portable biomedical microfluidics," *Lab on a Chip,* vol. 1, no. 10, pp. 80-85, 2010.

[11] D. Piwowar, "High Field Anymetric wareform for ulta-enhanced electroosmtic pumping of porous anodic alumina membrane," *Microfluidics and Nanofluidics,* vol. 6, no. 15, pp. 1-12, 2013.

[12] R. Probstein, Physicochemical Hydrodynamics, 2nd ed., New York: Wiley-Interscience Publication, 1994.

[13] R. J. Hunter, Zeta Potential in Colliod Science: Principals and Applications, London: Achedemic Press, 1981.

[14] H. C. Chang and L. Y. Yeo, Electrokinetically Driven Microfluidics and Nanofluidics, New York: Cambridge University Press, 2010.

[15] S. Lavine, J. R. Marriott, G. Neale and N. Epstien, "Theory of Electrokinetic Flow in Fine Capillaries at High Zeta Potentials," *Journal of Colliod and Interface Science,* vol. 52, no. 1, pp. 136-149, 1975.

[16] C. L. Whitehead and R. Rice, "Electrokinetic Flow in a Narrow Cylindrical Capillary," *The Journal of Physical Chemistry,* vol. 69, no. 11, pp. 4017-4024, 1965.

[17] D. J. Laser, A. M. Myers, S. Yao, K. F. Bell, K. E. Goodson and J. G. Santiago, "Silicon electroosmotic micropumps for integrated circuit thermal management," in *12th internaitonal Conference on Solid State Sensors, Actuators, and Microsystems*, Boston, 2003.

[18] E. V. Dose and G. Guiochon, "Timescales of Transient Process in Capillary Electrophoresis," *Journal of Chromatography A,* Vols. 263-275, no. 1, p. 652, 1997.

[19] D. J. Laser, K. E. Goodson, J. G. Santiago and T. W. Kenny, "High-frequency Actuation with Silicon Electroosmotic Micropumps," Dpt. of Mechanical Engineering, Stanford University, Stanford, CA, 2002.

[20] Y. F. Chen, M. C. Li, Y. H. Hu, W. J. Chang and C. C. Wang, "Low-Voltage Electroosmotic Pumping using Porous Anodic Alumina Membranes," *Microfluid Nanofluid,* vol. 5, no. 2, pp. 235-244, 2007.

[21] K. Daejoong, J. D. Posner and J. G. Santiago, "High flow rate per power electroosmotic pumping using low ion desnity solvents," *Sensors and Actuators A,* no. 141, pp. 201-212, 2007.

[22] Z. Xu, J. Miao, N. Wang, W. Wen and P. Sheng, "Digital flow control of electroosmotic pump: onsager coefficiencts and interfacial perameters determination," *Solid State Communications,* vol. 151, pp. 440-445, 2011.

[23] L. H. Olsen, H. Bruus and A. Ajdari, "AC electrokinetic micropumps: The effect of geometrical confinement, Faradaic current injection,," *Physical Review,* vol. 5, no. 73, 2006.

[24] E. Generalic, "Croatian-English Chemistry Dictionary & Glossary," 22 February 2015. [Online]. Available: http://glossary.periodni.com. [Accessed 22 June 2015].

[25] B. J. Kirby and E. F. Hasselbrink, "Zeta potential of micrfluidic subsrtrates: 1. Theory, experimental techniques, and effects on seperations," *Electrophoresis,* no. 25, pp. 187-202, 2004.

[26] S. Yao, D. E. Hertzog, S. Zeng, J. C. Mikkelsen Jr. and J. G. Santiago, "Porous glass electroosmotic pumnps: design and experiments," *Colloid and Interface Science,* vol. 268, pp. 143-153, 2003.

[27] M. E. Tawkfik and F. J. Diez, "On the relation between onset of bubbl nucleation and gas supersaturation concentration," *Electrochemica Acta,* no. 146, pp. 792-797, 2014.

[28] B. C. Donose, F. Harnisch and E. Taran, "Electrochemically produced hydrogen bubble probes for gas evolution kinetics and force spectroscopy," *Electrochemistry Communications,* no. 24, pp. 21-24, 2012.

[29] J. Posner, K. Salloum, M. Lebi, M. Reed, D. Buermann, M. Hage, B. Heiner and R. Kain, "Electroosmotic Pump with Improved Gas Management". US Patent 0187115, 29 July 2010.

[30] C. Lin, S. Yao, J. D. Posner, A. M. Myers and J. G. Santiago, "Toward orientation-independant design for gas recombination in closed-loop electroosmotic pumps," *Sensors and Actuators B,* no. 128, pp. 334-339, 2007.

[31] R. Vendetti, X. Xuan and D. Li, "Experimental characterization of the temperature dependance of zeta potential and its effect on electyoosmotic flow velocity in microchannels," *Microfluid Nanofluid,* no. 2, pp. 493-499, 2006.

[32] A. Brask, J. P. Kutter and H. Bruus, "Long-term stable electroosmotic pump with ion exchange membranes," *Lab on a Chip,* no. 5, pp. 730-738, 2005.

[33] D. W. Arnold, P. H. Paul and J. S. Schoeniger, "Method for Elliminating Gas Blocking in Electroosmotic Pumping Systems". US Patent 6287440, 11 September 2001.

[34] Z. Cao, L. Yuan, Y. F. Liu, S. Yao and L. Yobas, "Microchannel plate electroosmotic pump," *Microfluid Nanofluid,* vol. 13, pp. 279-288, 2012.

[35] J. L. Snyder, J. Getpreecharsawas, D. Z. Fang, T. R. Gaborski, C. C. Striemer, P. M. Fauchet, D. A. Borkholder and J. L. McGarth, "High performance, low-voltage electroosmotic pumps with molecularly thin silicon nanomembranes," *Proceedings of the National Academy of Sciences aof the United States of America,* vol. 10, no. 1073, 2013.

[36] J. A. Tripp, F. Svec, J. M. Frechet, S. Zeng, J. C. Mikkelsen and J. G. Santiago, "High-pressure electroosmotic pumps based on porous polymer monoliths," *Sensors and Actuators B,* no. 99, pp. 66-73, 2003.

[37] Q. Lu and G. E. Collins, "A fritless, EOF microchip pump for high pressure pumping aqueous and organic solvents," *Lab on a Chip,* no. 9, pp. 954-960, 2009.

[38] R. G. Newton and S. Davison, Conservation of glass, London: Butterworths, 1989.

[39] J. Miao, Z. Xu, X. Zhang, N. Wang, Z. Yang and P. Seng, "Micropumps based on the enhanced electroosmotic effect of aluminum oxide membrnaes," *Advanced Materials,* no. 19, pp. 4234-4237, 2007.

[40] C. P. D. K. K. Kwon, "High-flowrate, compact electroosmotic pumps with porous polymer track-etch membranes," *Sensorsd and Actuators,* no. 175, pp. 108-115, 2012.

[41] A. J. Bard and L. R. Faulkner, Electrochemical Methods: Fundementals and Applications, New York: John Wiley & Sonds Inc., 2001.

[42] M. E. Tawfik, T. E. Hansen and F. J. Diez, "The gas generation measurment at high electric field in electrokinetic devices," in *APS Division of Fluid Dynamics*, Pittsburgh, 2013.

[43] M. Vanagas, J. Kleperis and G. Barjars, "Water Electrolysis with Inductive Voltage Pulses," in *Electrolysis*, InTech, 2012, p. chapter 2.